CHAPTER 4 PETROGRAPHY AND MINERAL GEOCHEMISTRY

4.1 – PRIMARY MAFIC MINERALS

4.1.1. Olivine

Very few preserved olivine grains were encountered in the samples selected for the current investigation, as the study concentrates on the highly altered areas of the Complex. During a preceding reconnaissance study of the harzburgite and wehrlite layers in the LHZBG Unit on the farm Slaaihoek 540 – JT by the author, olivine was encountered in the form of both pristine and completely altered grains (Steenkamp, 2004). The grains encountered during the present investigation were all euhedral and well rounded. Most of the olivine grains examined show signs of alteration, such as cracks in the olivine showing signs of hydrothermal alteration that resulted in the formation of serpentine (lizardite) in contact with the preserved olivine along the edges of the cracks. Since all of the samples were collected at depths that have not suffered any surface weathering effects, it may be inferred that the alteration is due to either syn-magmatic or post-magmatic hydrothermal alteration events. In the central part of internal cracks, in contact with the serpentine, non-continuous stringers of secondary magnetite are sometimes developed (Figure 4.1). The secondary magnetite is formed by topo-metasomatic mobilization of iron oxide from the olivine.

The mineral chemistry of olivine grains encountered during this investigation, as analysed by microprobe, is tabulated and presented in Appendix 2.

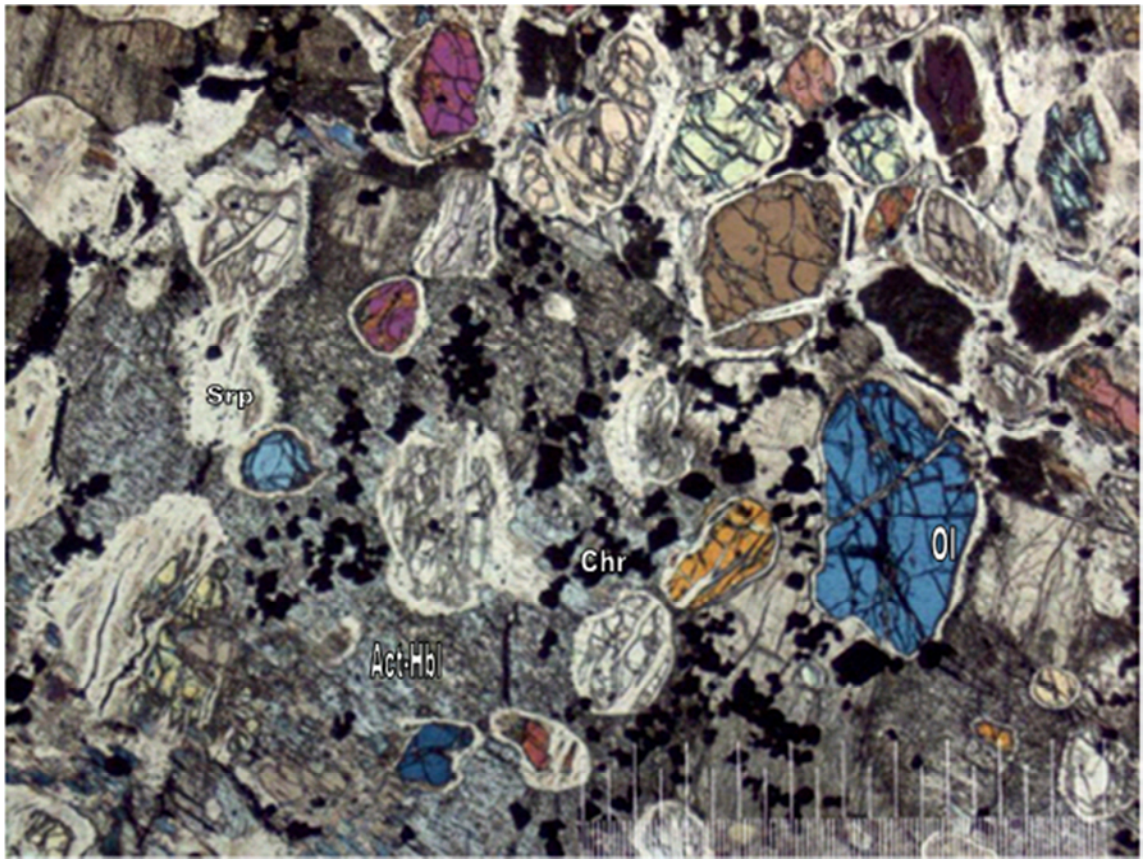

Figure 4.1. Euhedral to subhedral olivine (ol) grains that suffered hydrothemal metamorphism in the PCR Unit. Cracks in olivine grains are filled with serpentine (srp) and secondary magnetite stringers. Serpentine forms in haloes around olivine grains and partly replace them. Euhedral chromite (chr) grains (black) are found in association with the olivine. Olivine and chromite grains are poikilitically enclosed by clinopyroxene (diopside), hydrothermally altered to amphibole of actinolitic (act) to hornblende (hbl) composition. The picture scale bar is 1000. Taken with cross-polarised light. (Sample: UK12D).

In the LHZBG Unit, olivine grains are usually found in two associations. The first is as scattered grains in the harzburgite matrix, with an altered appearance as described above. These grains are poikilitically enclosed by diopside. Olivine grains are also found in the centre of triple junction points formed by larger clinopyroxene grains (Figure 4.2). The second association is in the wehrlite layers within the LHZBG Unit as rounded, euhedral grains surrounded by net-textured sulphides. Most of the olivines in the wehrlite layers have been partially or completely serpentinized and secondary magnetite is also found in and around these serpentinized olivine grains (Figure 4.3). Identifiable olivine grains in the

PCR Unit were only found in UK12, where their appearance is similar to the scattered olivine grains found in the LHZBG Unit (Figure 4.2).

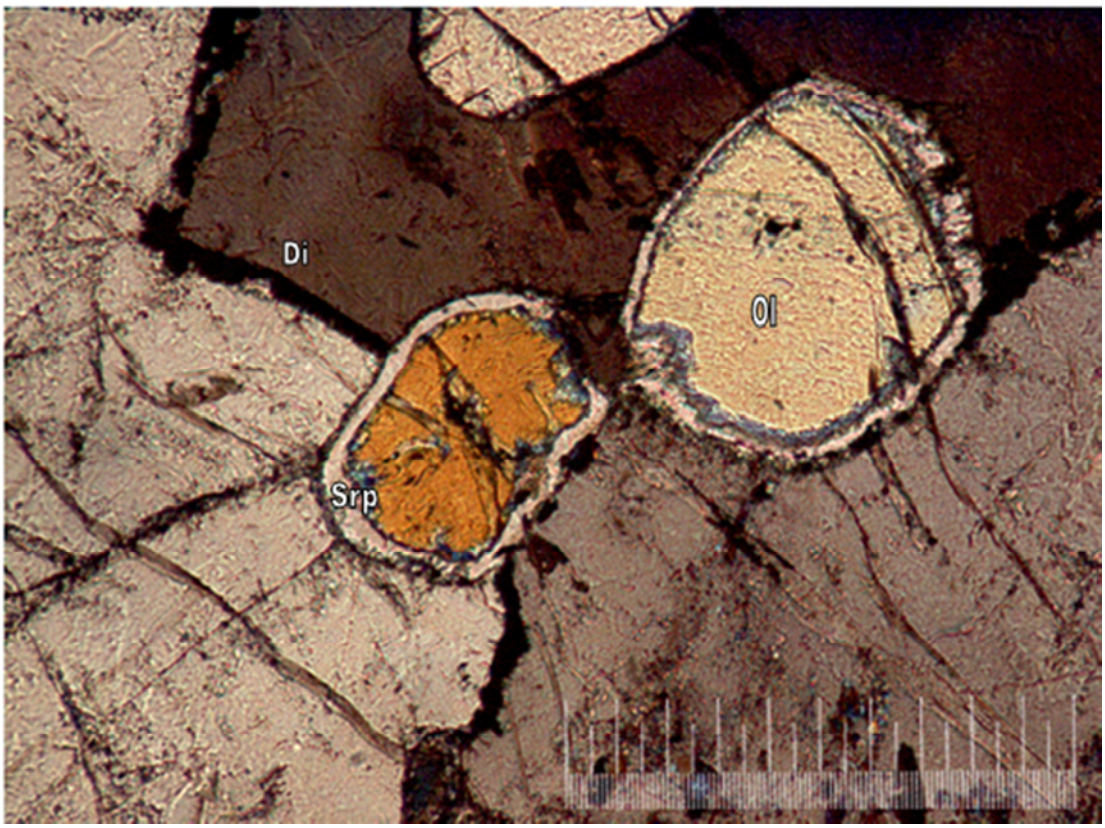

Figure 4.2. Rounded olivine (ol) grains with haloes of serpentine (srp) near a triple junction of diopside (di) grains, found in the LHZBG Unit. The picture scale bar is 1000 micron. Taken with cross-polarised light. (Sample; CS14).

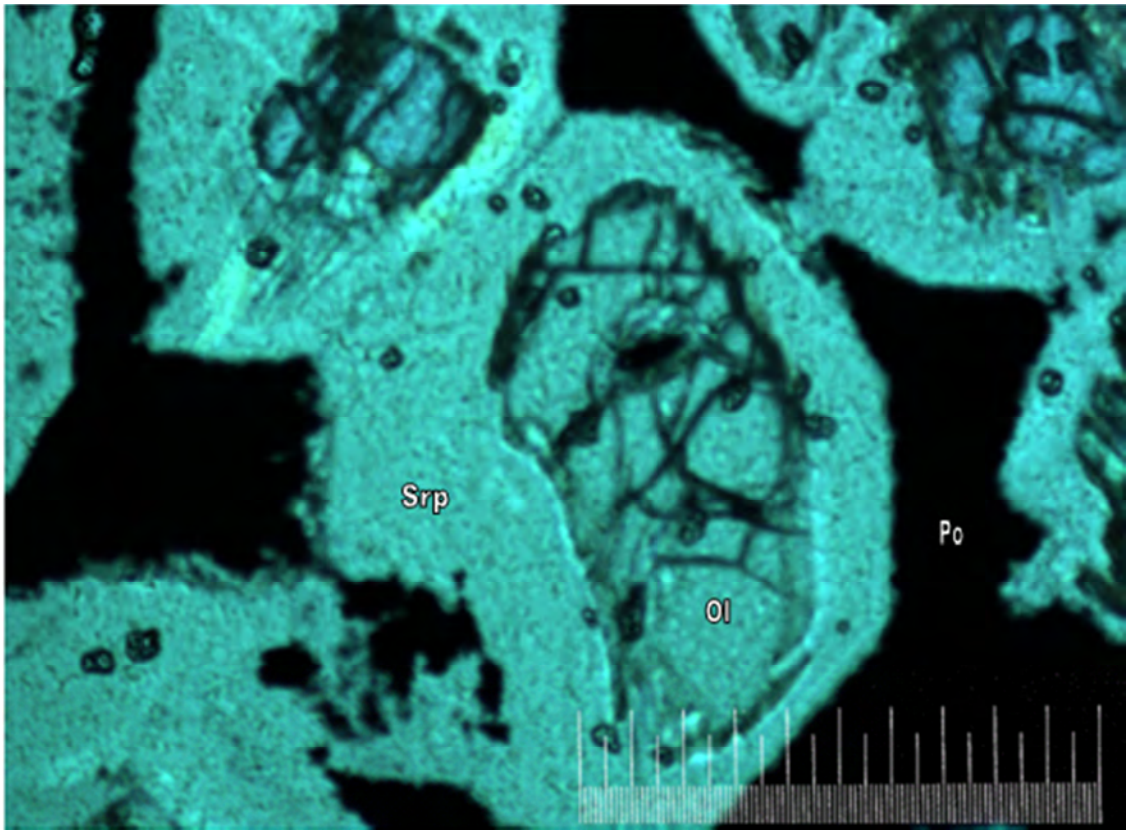

Figure 4.3. Olivine (ol) grains partially replaced by serpentine (srp), enclosed in net-texture sulphides (pyrrhotite – (po)) in the wehrlite layers found in the LHZBG Unit. The picture scale bar is 1000 micron. Taken with plane-polarised light. (Sample; CS 18).

Microprobe analyses (Appendix 2) of olivine grains revealed that the forsterite content of the olivines varies between $Fo_{75.78}$ and $Fo_{82.58}$, with an average of $Fo_{78.13}$ for the LHZBG Unit (n = 15), and between $Fo_{84.04}$ and $Fo_{95.48}$ in the PCR Unit (n = 34), with an average of $Fo_{88.15}$. There does not appear to be a significant difference between the compositions of olivine found in the wehrlite layers within the LHZBG Unit compared to that of the hybrid rock in the same unit. Olivine grains from both wehrlite and harzburgite in the LHZBG Unit contain between 0.1 and 0.23 % NiO and have magnesium numbers (Mg #) of between 0.64 and 0.73 (n = 15). The olivine grains analysed from the PCR Unit contain between 0.01 and 0.17 % NiO and have Mg # values ranging between 0.84 and 0.95 (n = 34).

Figure 4.4 gives a NiO versus Fo % graph showing that the olivine grains analysed from the PCR Unit have a higher forsterite content than olivine grains from the LHZBG Unit. The olivine from the LHZBG Unit has a higher NiO content compared to olivine from the PCR Unit. There are also two groups of olivine compositions in the PCR, one with on average less NiO and has a higher Fo-content and a second with a slightly higher average NiO content and has a lower Fo-content. Both varieties are found in samples with a diopside matrix that has suffered hydrothermal alteration, resulting in partial ampibolisation and chloritisation of the diopside crystals.

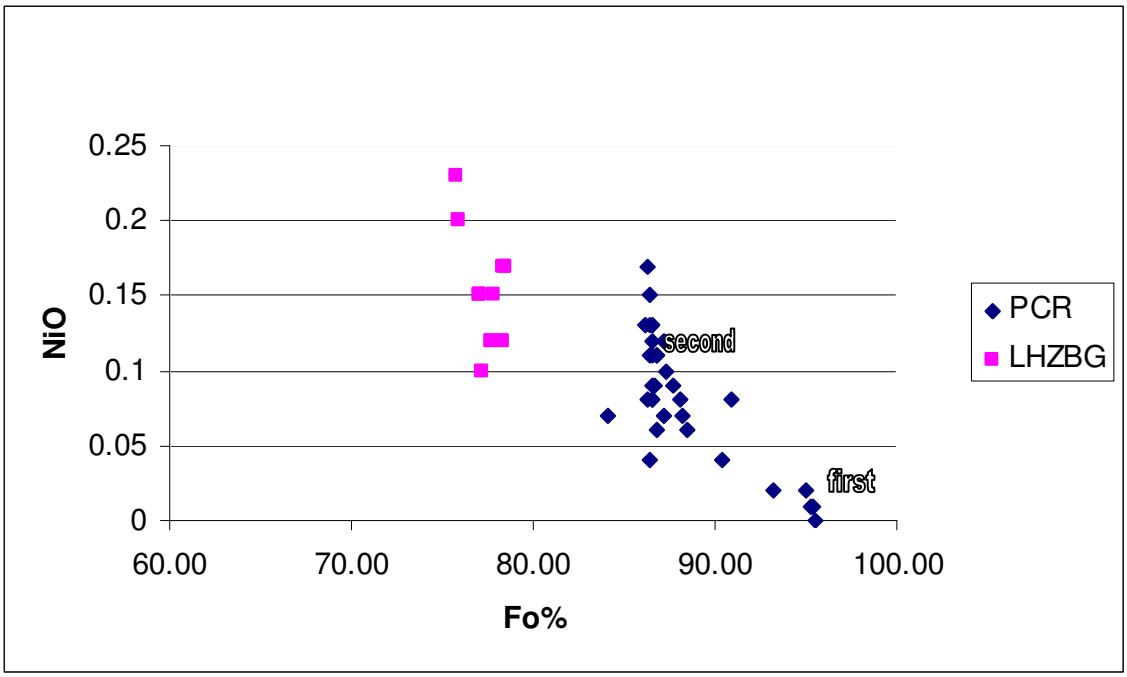

Figure 4.4. Comparison of olivine grain compositions of the LHZBG and PCR Units, based on NiO-content and the percentage forsterite. Data in Appendix 2.

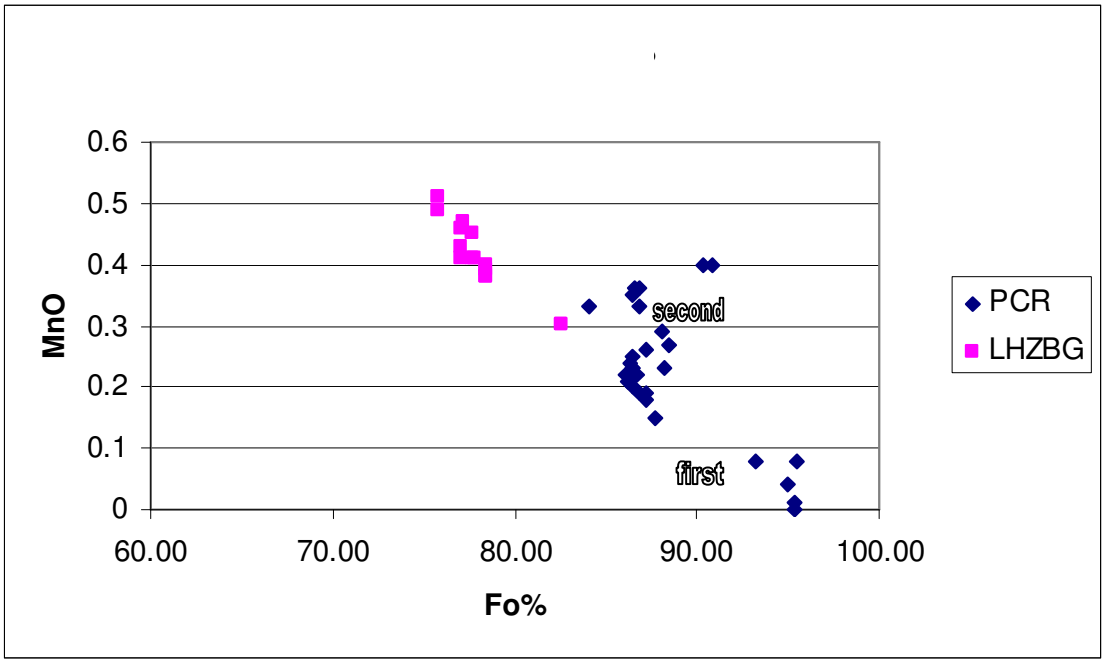

Figure 4.5. Comparison of olivine from the LHZBG and PCR Units on a MnO versus forsterite content diagram. Data in Appendix 2.

From figure 4.5 it may be seen that the olivines from the LHZBG Unit have on average a higher MnO content compared to olivines from the PCR. The two groups of olivine in the PCR Unit identified in Figure 4.4 are also distinguishable in this diagram. The first has a lower MnO content and higher Fo-content and the second a slightly higher MnO content but lower Fo-content.

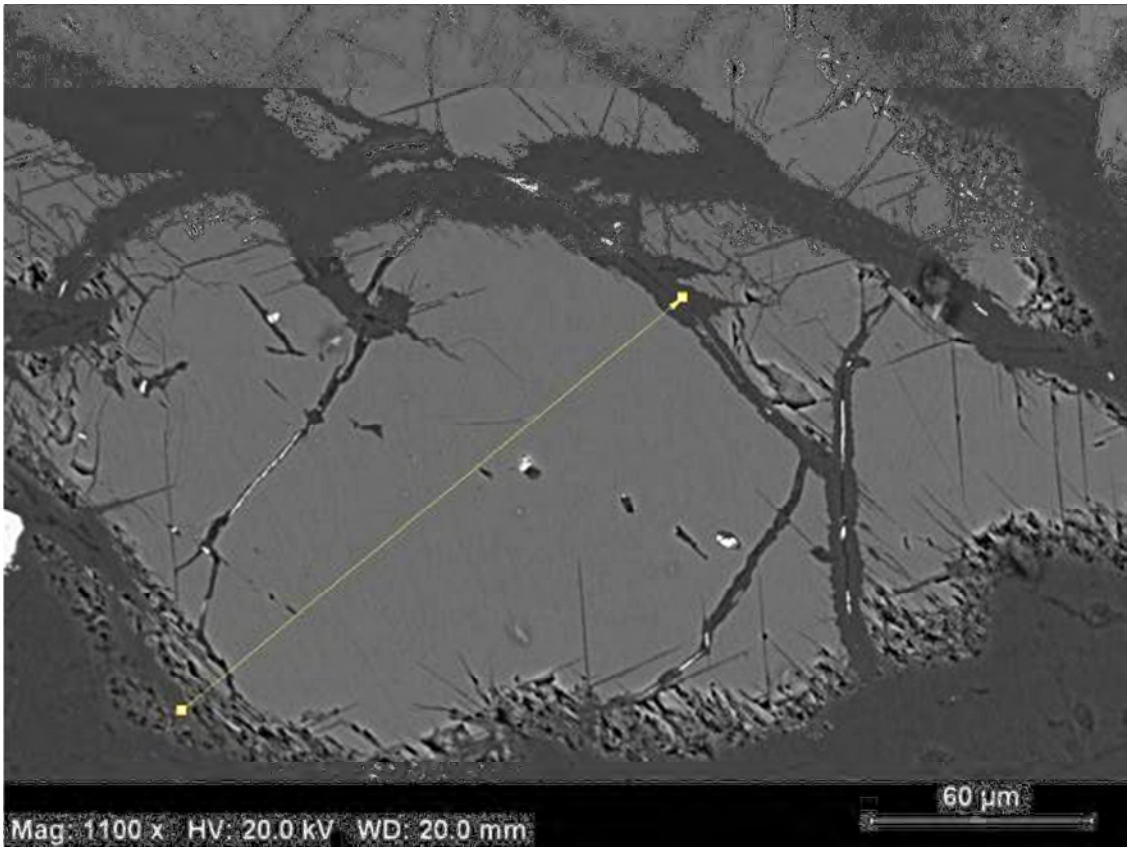

Figure 4.7. Backscatter image of olivine (light grey) with a line indicating the position of a line scan. (Sample: UK12D). Image by P.Graser.

Line scans were performed to determine zonation in the olivine grains, and to determine the effect of hydrothermal alteration or metasomatism of the elements close to and in the affected areas. Figure 4.7 is a backscatter image of an olivine grain tested for zonation.

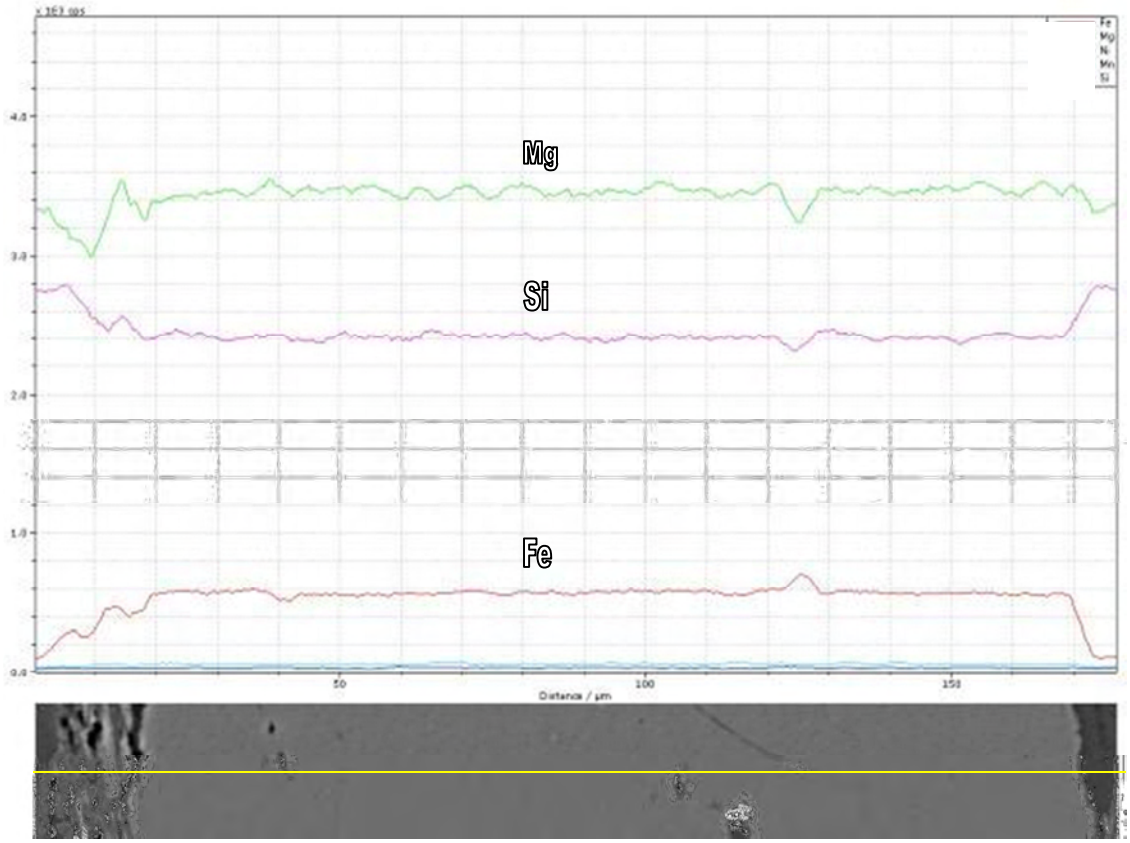

Figure 4.8. Elemental distribution of Mg (top), Si (centre) and Fe (bottom) in line scan of olivine. (Sample; UK12D). Image P.Graser.

In Figure 4.8, it may be seen that the olivine grain shows no evidence of zonation. The increase and decrease of elements on the edges is interpreted as indications of no hydrothermal alteration at the rim of the olivine grain. The depression in the Mg and Si and spike of Fe lines on the grain is most likely an artifact due to the visible scratch. The higher level of Si (purple line, centre) on the rim relative to the rest of the grain is probably due to the formation of serpentine. There is slight depletion of Mg (green line, top) relative to the grain on the edges.

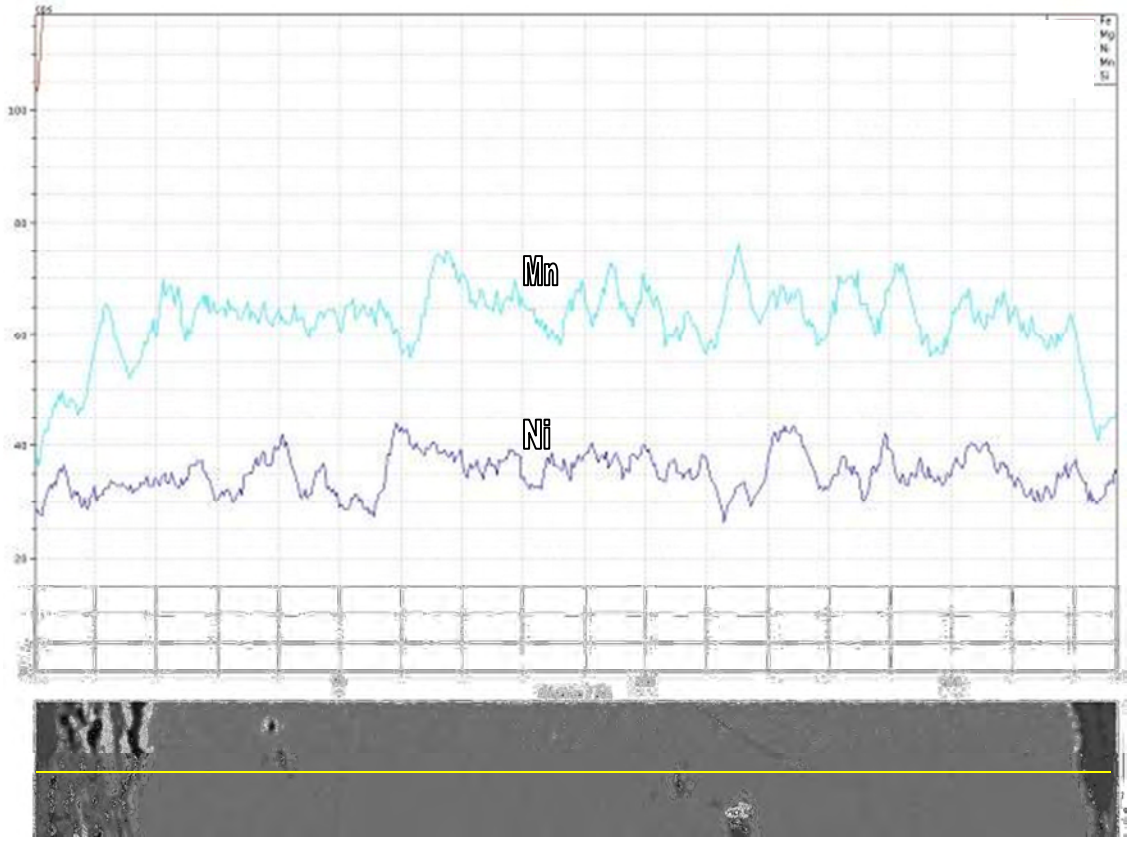

Figure 4.9. Elemental distributions of Mn (top) and Ni (bottom) in line scan of olivine grain. (Sample; UK12D). Image P.Graser.

The greater degree in variation in elemental concentrations is probably "analytical noise" due to lower concentrations of the two minor elements analysed. Slight variations in Mn and Ni content can be seen in Figure 4.9. Although some peaks and dips occur sympathetically, there is no systematic correlation. The Mn content depletes steeply towards the rims. The Ni content on the other hand remains fairly constant, indicating the less mobile nature of Ni.

All the olivine grains that line scans were performed on showed no zonation, suggesting that the olivine was crystallized from a single melt and was not subject to the effects of later pulses.

4.2 Pyroxene

4.2.1 Clinopyroxene and orthopyroxene

The samples studied during the previous reconnaissance of the harzburgite and wehrlite layers from the LHZBG on the farm Slaaihoek showed that the clinopyroxene mineral present is diopside, whereas the orthopyroxene has the composition of enstatite (Steenkamp, 2004). In this early investigation, two types of clinopyroxene were recognized, the first a diopside of magmatic origin and the second a diopside of metamorphic/metasomatic origin. This identification was based on the textural differences and different Cr-contents (Steenkamp, 2004).

A distinction is made here between the three geological environments in which pyroxenes are found in the rocks of the Complex. The first is orthopyroxene and clinopyroxene found in the wehrlite layers and thought to represent the primary magmatic mineralogy. The second is in the harzburgite and hybrid rocks, referred to as pyroxenites. The third is pyroxene (diopside and fassiate) found in the calc-silicate xenoliths. The orthopyroxene grains analysed during this investigation fall in the enstatite composition field, similar to those analysed in the previous project.

Diopside is the main clinopyroxene encountered in the samples analysed. The diopside texturally displays triple junction points in some sections. Some of the diopside from the LHZBG Unit, as well as that from xenoliths, plot above the diopside-hedenbergite (Di-Hb) line (Figures 4.12, 4.13 and 4.16) and indicate that these diopside grains may be of a metamorphic/metasomatic origin. Uralitization of the pyroxene grains is considered to be the result of pneumatolytic action by the water-enriched residual magmatic fluid on the grains (Deer et al., 1992). The pyroxene grains inferred to be of magmatic origin have rounded edges or embayments which may indicate thermal, chemical or mechanical erosion. The analytical results considered here pertain to microprobe analyses done during this investigation. These results are presented in Appendix 2.

The diopside grains in the harzburgites from the talc-rich study area occur in association with olivine and chromite grains, and poikilitically encloses these two minerals (Figure 4.10). In contrast to the findings reported by van Zyl (1996), no poikilitic enstatite grains were encountered in the current investigation. Both enstatite and diopside crystals have been uralitized to the same extent in the LHZBG and the PCR Units and are also associated with secondary minerals, including actinolite-tremolite, hornblende, chlorite, serpentine and secondary magnetite.

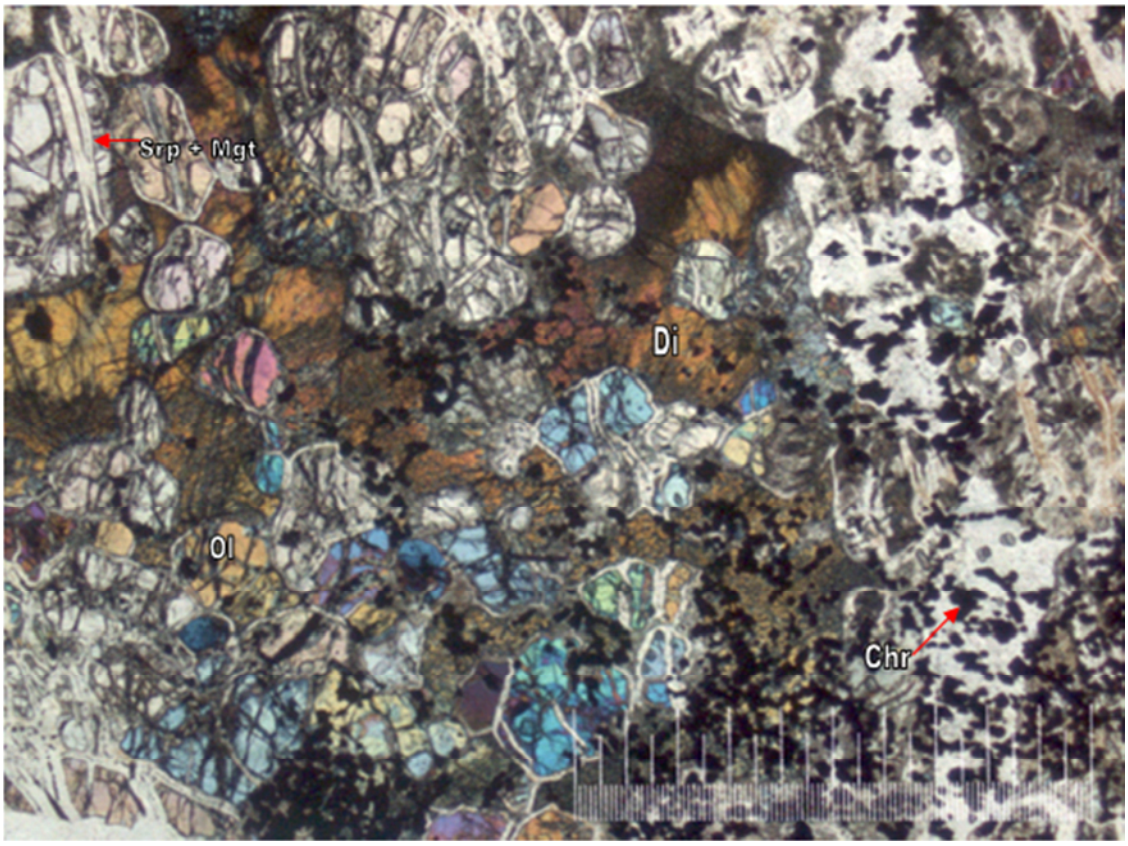

Figure 4.10. Diopside (Di) poikilitically enclosing partially serpentinized (srp) olivine (ol) grains with non-continues secondary magnetite (mgt) stingers and euhedral chromite (chr) grains. This sample is from the PCR Unit. The picture scale bar is 1000 micron. Taken with cross-polarised light. (Sample; UK12G).

The diopside in different varieties of calc-silicate xenoliths is found in association with other minerals formed by thermal metamorphism and metasomatism (Figure 4.11). The xenoliths from borehole UK3 (samples N, Q and U) consist mainly of diopside and calcite

with minor actinolite and chlorite. Xenoliths from borehole SH176 consist of diopside and calcite, but also contain significant amounts of grossular garnet. Calcite is absent from the xenoliths from sample UK12I, but this sample contains significant amounts of plagioclase and minor amounts of muscovite, actinolite and chlorite. This latter variety of xenolith is refered to as a "contaminated" xenolith, as discussed in Chapter 7. Calcite is also absent from the xenolith in sample UK48G, where as it contains significant amounts of epidote and minor actinolite, chlorite and pyrite.

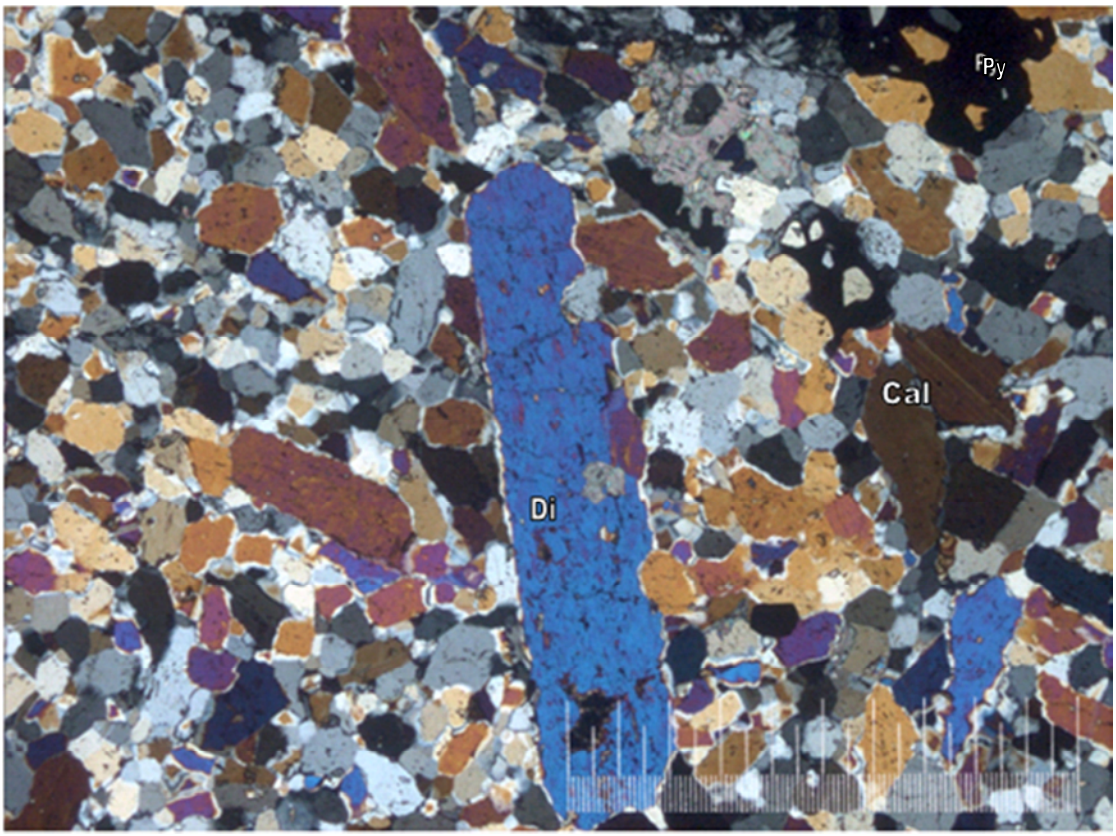

Figure 4.11. Diopside grains in a calc-silicate xenolith from the LHZBG Unit. The minerals depicted are diopside (di), calcite (cal) and pyrite (py). The picture bar scale is 1000 microns. Taken with cross-polarised light. (Sample: CS21H).

The pyroxene compositions determined for this study area can be plotted in various diagrams to characterize them. The pyroxene composition of all the grains analysed are plotted according to AMI-standards as put forward by Morimoto (1989).

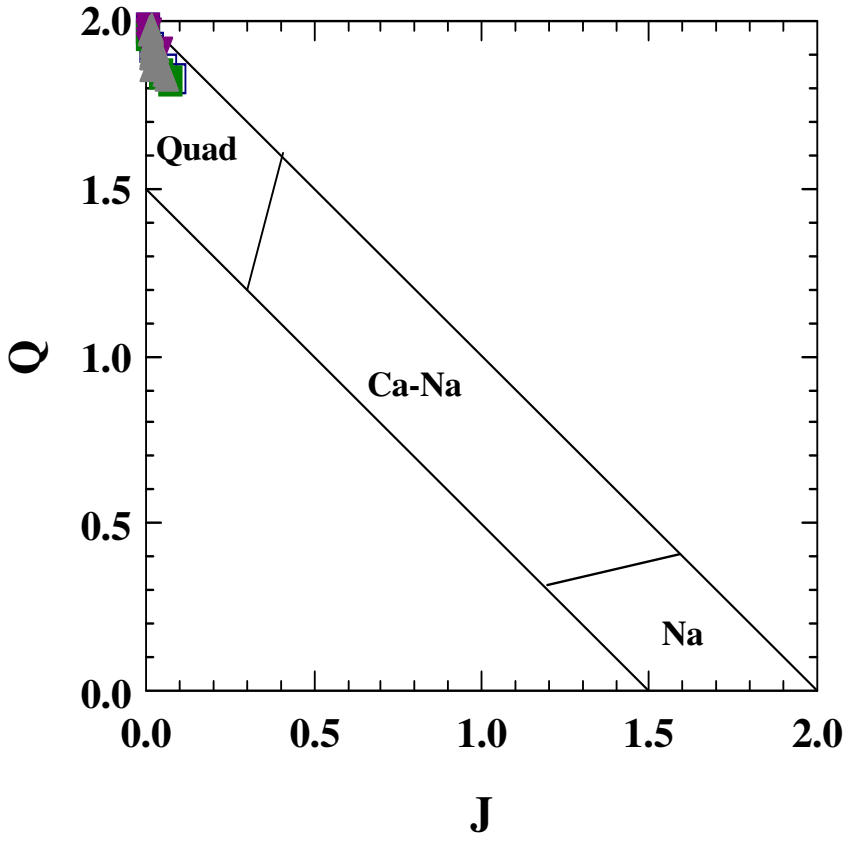

Figure 4.12. Microprobe analyses of pyroxenes from the PCR and LHZBG Units plotted on a Q-J diagram, where Q = Ca + Mg + Fe^{2+} and J = 2Na (After Morimoto, 1989). The legend is the same as presented in Figure 4.13 and 4.14.

Pyroxenes from the PCR and LHZBG Units plot in a tight cluster in the calcium quadrilateral field (Figure 4.12).

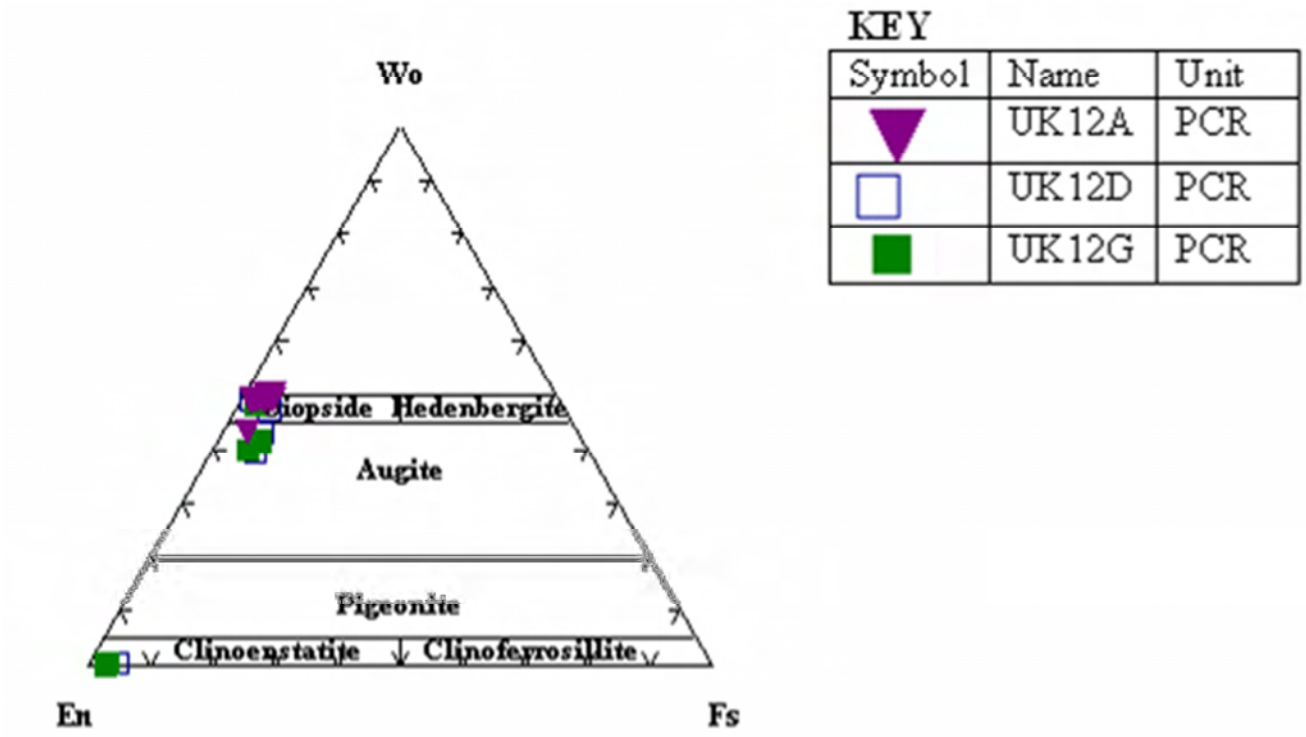

Figure 4.13. Plot of pyroxene minerals from the PCR Unit in the Wo-En-Fs system (After Morimoto, 1989).

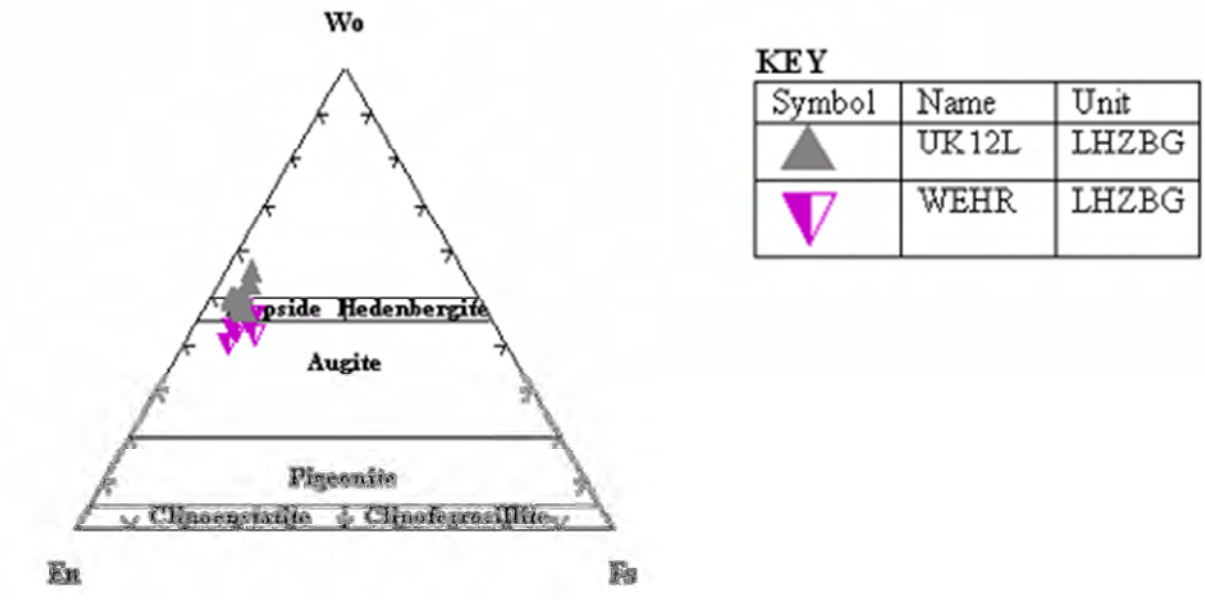

Figure 4.14. Plot of pyroxene minerals from the LHZBG Unit in the Wo-En-Fs system (After Morimoto, 1989).

The graphed data show that pyroxene grains analysed belong to two compositional varieties, diopside and enstatite. The grains of the two types are individually very similar in composition as is demonstrated in Figures 4.13 and 4.14. Pyroxenes from the PCR (Figure 4.13) and LHZBG Units (Figure 4.14) are plotted. In addition, the compositions of the clinopyroxene grains from the wehrlite layers, found in the LHZBG on the farm Slaaihoek 540 - JT, sampled during the previous reconnaissance (Steenkamp, 2004) have been added for comparative purposes (Figure 4.14). During the reconnaissance investigation it was determined that the clinopyroxenes from the parapyroxenites in the LHZBG Unit on the farm Slaaihoek 540 - JT fall in the diopside-augite field and the orthopyroxenes fall in the enstatite field. The wehrlite layers contain clinopyroxene that fall in the diopside-augite field (Figure 4.14).

Pyroxene, analysed from the PCR Unit sampled on the farm Uitkomst 541 - JT, plots in the clinopyroxene and orthopyroxene fields (Figure 4.13). The orthopyroxene falls into the enstatite field and the clinopyroxenes fall into the augite and diopside fields. Clinopyroxene from the upper and central parts of the LHZBG Unit on Uitkomst also plots (Figure 4.14) both the augite and diopside fields, while the clinopyroxenes from the lower part of the unit (near the basal contact) only plot (Figure 4.14) in the diopside field and above the diopside-hedenbergite tie-line.

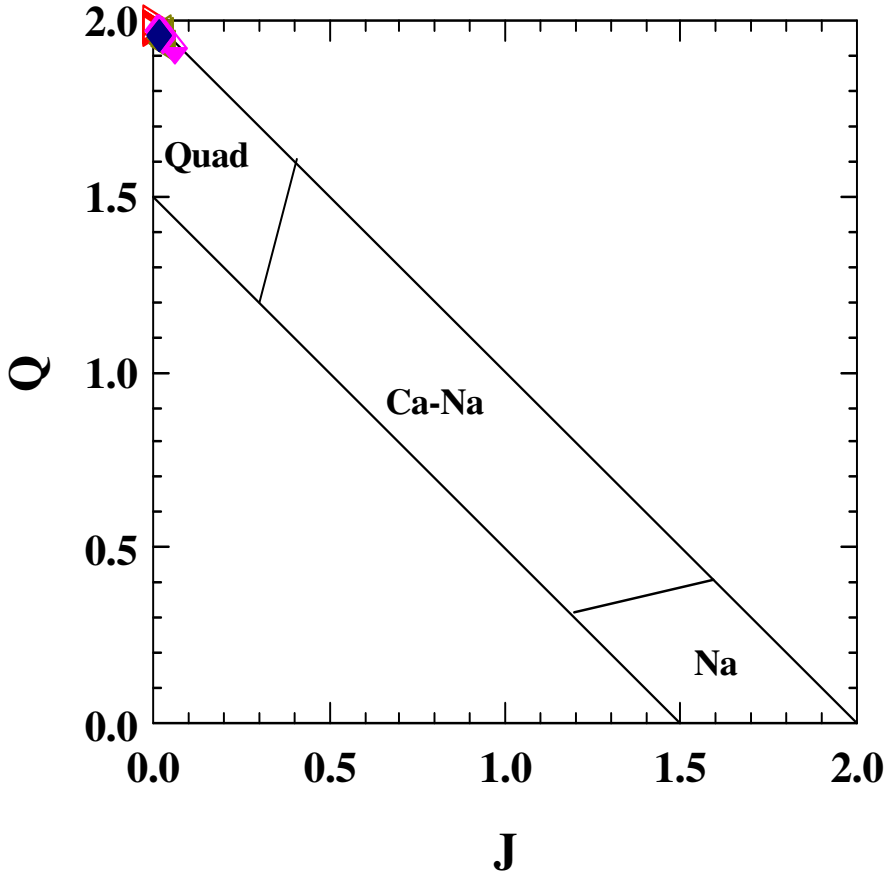

Figure 4.15. Plot of pyroxene compositions in xenoliths, on the Q-J diagram (After Morimoto, 1989). The legend is the as for Figure 4.19.

Pyroxene grains from the xenoliths plots in a very tight cluster in the quadrilateral field of the Q-J diagram (Figure 3.15).

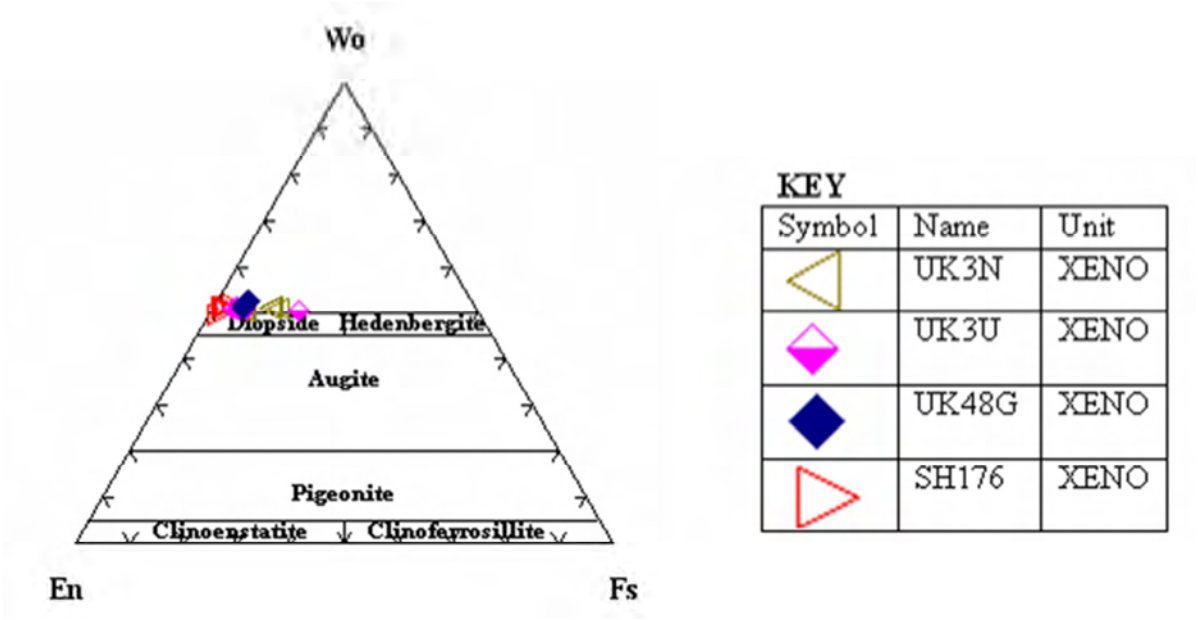

Figure 4.16. Plot of pyroxene compositions of xenoliths in the Wo-En-Fs system (After Morimoto, 1989).

In Figure 4.16 it can be seen that the xenoliths contain no orthopyroxene. The composition of all the grains plot in the diopside field, close to and slightly above the Di-Hb tie-line.

According to Deer et al., (1992) the structure of pyroxene can be expressed in the following way: M2 M1 T_2O_6, where M2 and M1 refer to cations in generally distorted and regular octahedral coordination positions respectively. T refers to tetrahedrally coordinated cations. The composition of Mg-Fe and Ca pyroxenes can be represented by the formula: $M2(R2^{+})M1(R^{2+})T(2R^{4+})O_6$. Based on the assumption that more than one R^{4+} cation is present in T sites, the composition of pyroxene containing monovalent and trivalent cations can be described in terms of coupled substitutions. Where $M1(R^{3+})T(R^{3+})$ produces end-member conditions it is commonly termed the "Tschermak" component. In natural minerals the amount of Al in T sites is normally limited to ~0.5. Harris and Chaumba, (2001) ascribe the composition of diopsides found at Sandsloot (PPRust), plotting above the Di-Hb line, as being due to the presence of Al in octahedral sites and that Ca does not exceed one cation per six oxygens. A possible means of formation is given below in the following reactions.

i) $4CaCO_3 + (6CaAl_2Si_2O_8 + 4Mg_2SiO_4) = 4CalAl_2SiO_6 + 6CaMgSi_2O_6 + 2\ MgAl_2O_4 + 4\ CO_2$

calcite + anorthite + forsterite CaTs-pyx + diopside + spinel

ii) $CaMg(CO_3)_2 + 2\ CaAl_2Si_2O_8 + Mg_2SiO_4 = CaAl_2SiO_6 + 6CaMgSi_2O_6 + MgAl_2O_4 + 2CO_2$

dolomite + anorthite + forsterite = CaTs-pyx + diopside + spinel

However, olivine and plagioclase are lacking in the samples analysed. It has been shown by Weeks (1956b quoted in Deer et al., 1992) that diopside may form at temperatures lower than forsterite where the P_{CO2} is below 1000 atm. according to the following reaction :

$CaMg(CO_3) + SiO_2 = CaMgSi_2O_6 + 2CO_2$

Dolomite + Quartz = Diopside + Carbon dioxide

The occurrence of a non-quadrilateral component, namely CaTs-pyroxene (Ca-Tschermak molecule) has been reported in significant amounts both where assimilation of dolomites took place (e.g. Ioko-Dovyren) and at various limestone-magma contacts (e.g. Abu El-Enen et al., 2004). An increase in the Ca-Tschermak component from the core of clinopyroxene grains to the edge indicates a decrease in silica saturation due to concomitant prograde decarbonation reactions that generally consume SiO_2 (Povoden et al., 2002).

The clinopyroxene that falls above the hedenbergite-diopside line and are described by Gilg et al., (2001) as a subsilicic ferroan aluminian diopside (fassaite) with significant Ca-Al-Tschermak exchange components. Fassaite is a Ca and Al-rich pyroxene found in metamorphosed dolomite and limestone.

4.2.2 Comparison of Pyroxene Compositions in the Uitkomst Complex

Meaningful information is obtained by comparing the compositions of pyroxene grains from different locations and lithological association. Slaaihoek refers to the pyroxene found in the samples from the farm Slaaihoek, and Uitkomst refer to the pyroxene found in samples from the farm Uitkomst. The wehrlite samples are derived from the Slaaihoek section. All comparisons are relative to Ca-content, this provides a very prominent distinction between the species.

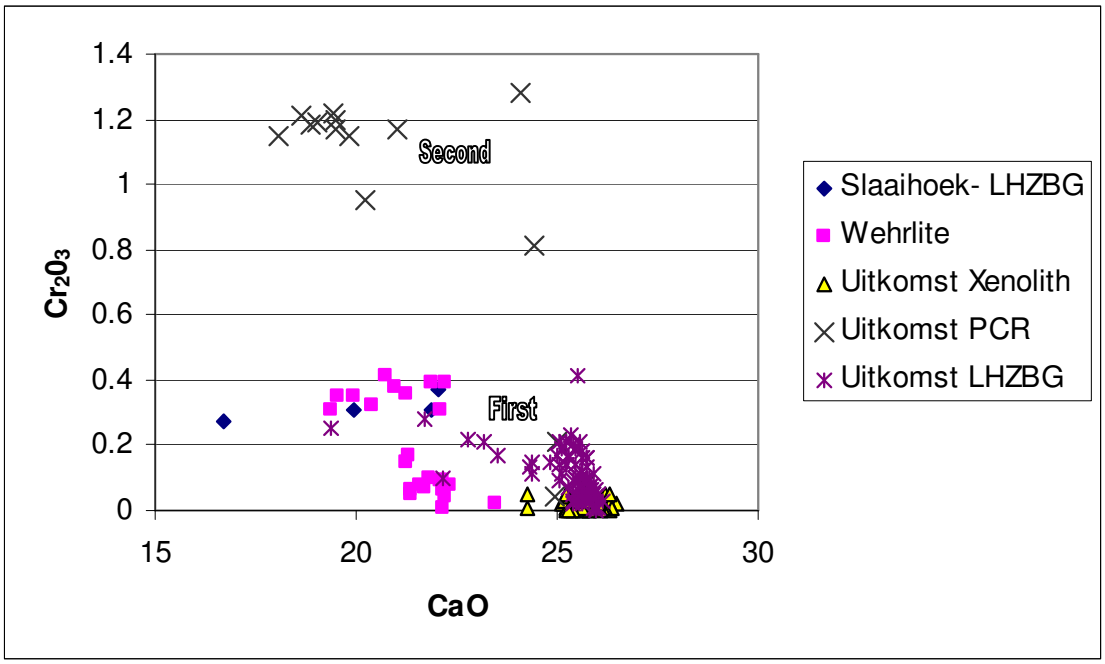

Figure 4.17. Clinopyroxene species from the Uitkomst Complex based on the differences in Cr_2O_3 content of the samples analysed.

There are two distinct groups of clinopyroxene, based on Cr content. The diopside in the PCR Unit is enriched in Cr relative to the clinopyroxenes from the LHZBG Unit's, harzburgite, wehrlite and xenoliths (Figure 4.17) respectively.

There are two species of clinopyroxene present in the wehrlite layers, the first slightly more depleted in Cr than the second. However, the margin of error on analyses and small

difference in content does not make it a diagnostic feature. Diopsides from the LHZBG Unit on Uitkomst 541 - JT and the Uitkomst calc-silicate xenoliths have similar Ca content. The Uitkomst LHZBG clinopyroxenes have higher Cr contents, whereas those from within the xenoliths contain little to no Cr. Some of the Uitkomst LHZBG clinopyroxene grains show an increase in their Cr-content with a decrease in the Ca-content. These Uitkomst LHZBG clinopyroxene compositions tend towards the composition of clinopyroxenes of the Slaaihoek pyroxenites with the Cr-rich clinopyroxene grains present in the wehrlite, being somewhat "transitional" between them.

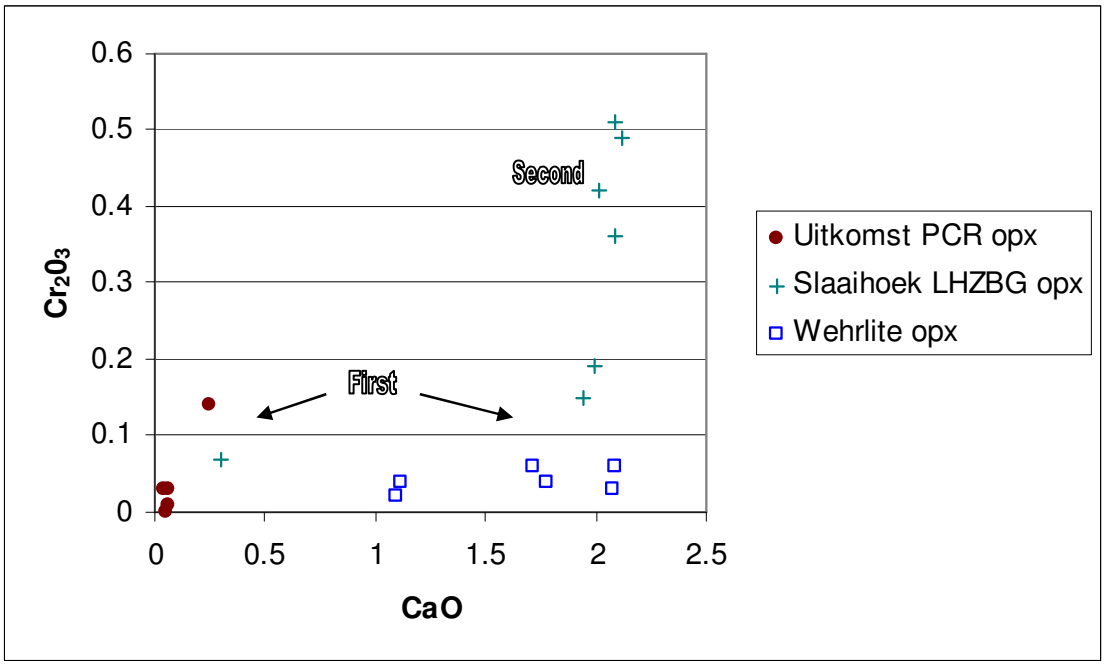

Figure 4.18. Orthopyroxene species from the Uitkomst Complex based on the differences in Cr_2O_3 content of the samples analysed.

The Slaaihoek harzburgite contains two orthopyroxene (enstatite) species (Figure 4.18), the first with a lower Cr-content and the second with a slightly higher Cr-content. The orthopyroxene from the Uitkomst PCR harzburgites and from the wehrlite layers fall in the low Cr-content range of enstatite. The Slaaihoek section samples fall in both. The difference in composition and analytical margin of error may exclude this as a diagnostic

feature. The Cr-content in both ortho- and clinopyroxene in the Slaaihoek samples are higher relative to the Uitkomst section samples.

In Figure 4.19 all the clinopyroxenes analysed form the Uitkomst Complex are compared in a MnO versus CaO diagram. The same comparison for orthopyroxene is made in Figure 4.23.

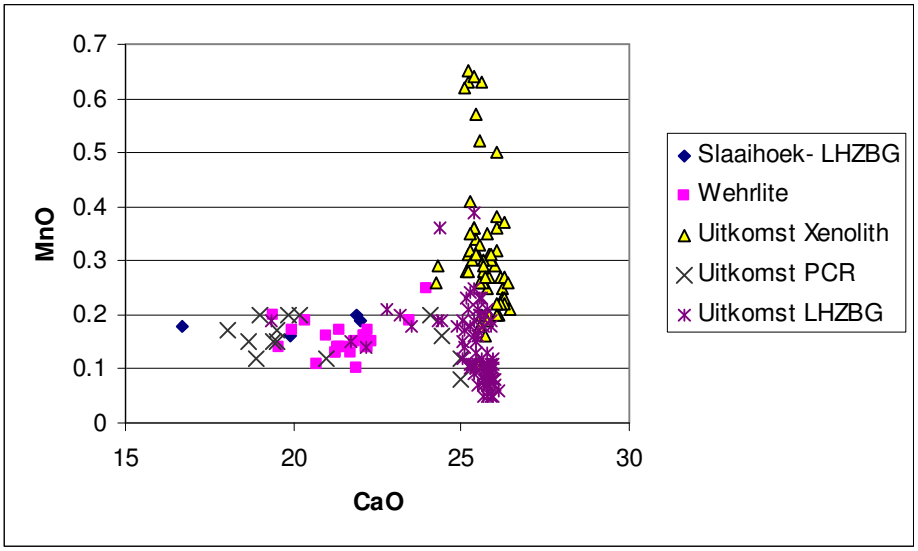

Figure 4.19. MnO against CaO content in clinopyroxene samples from the Uitkomst Complex analysed.

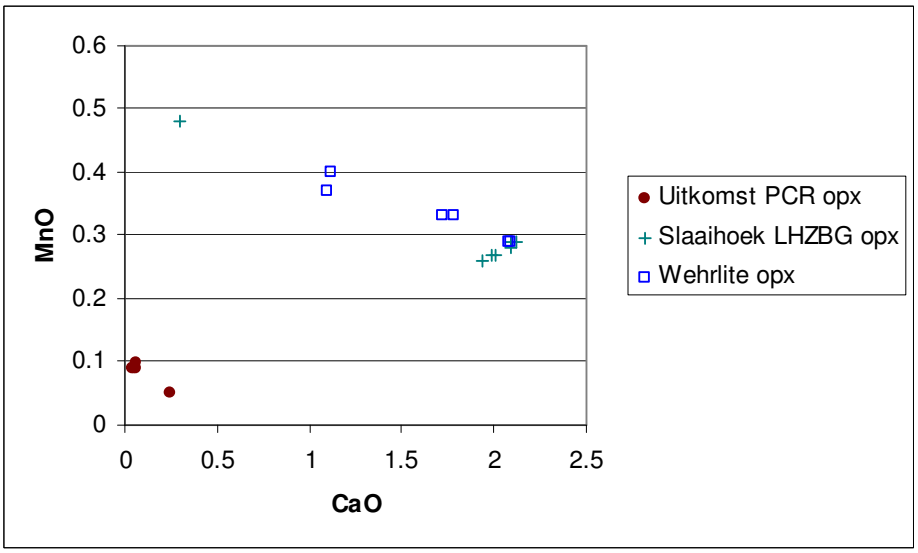

Figure 4.20. MnO against CaO content in orthopyroxene samples from the Uitkomst Complex analysed.

The fassaite diopside (labelled Uitkomst Xenolith) grains from the xenoliths (Figure 4.19) appear to be more MnO enriched relative to the other diopside occurrences. There also appear to be two species of diopside present in the xenoliths, the first with a slightly higher MnO content than the second. The clinopyroxenes found in the Slaaihoek harzburgites, the wehrlite layers and the PCR harzburigites (Figure 4.19) have a lower concentration of CaO relative to the Uitkomst clinopyroxenes, but show approximately the same range of MnO content. There appear to be a "transitional" component between the clinopyroxene composition of the Uitkomst LHZBG and PCR analysed samples. The enstatite (orthopyroxene) grain analyses (Figure 3.20) shows a general trend in the wehrlite and Slaaihoek LHZBG samples. These grains have a slightly higher MnO content relative to the samples from Uitkomst LHZBG (Figure 4.20). However, the compositional difference is again small and considering analytical error, also not considered a diagnostic feature.

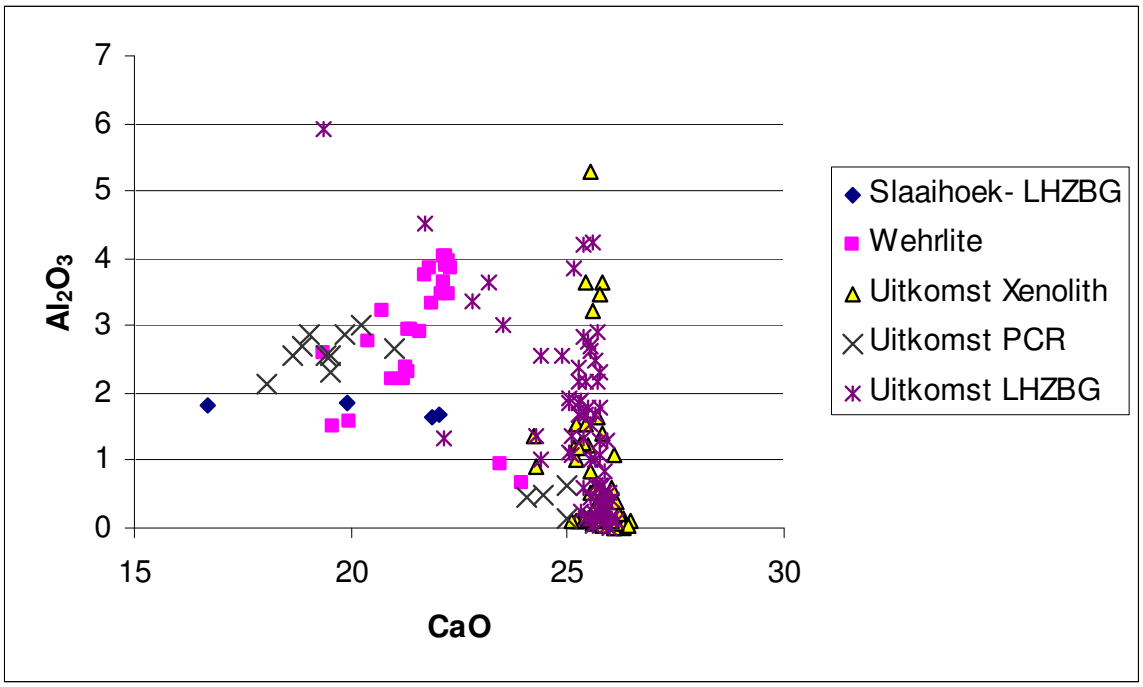

Figure 4.21. Al_2O_3 against CaO contents of clinopyroxenes analysed from the Uitkomst Complex.

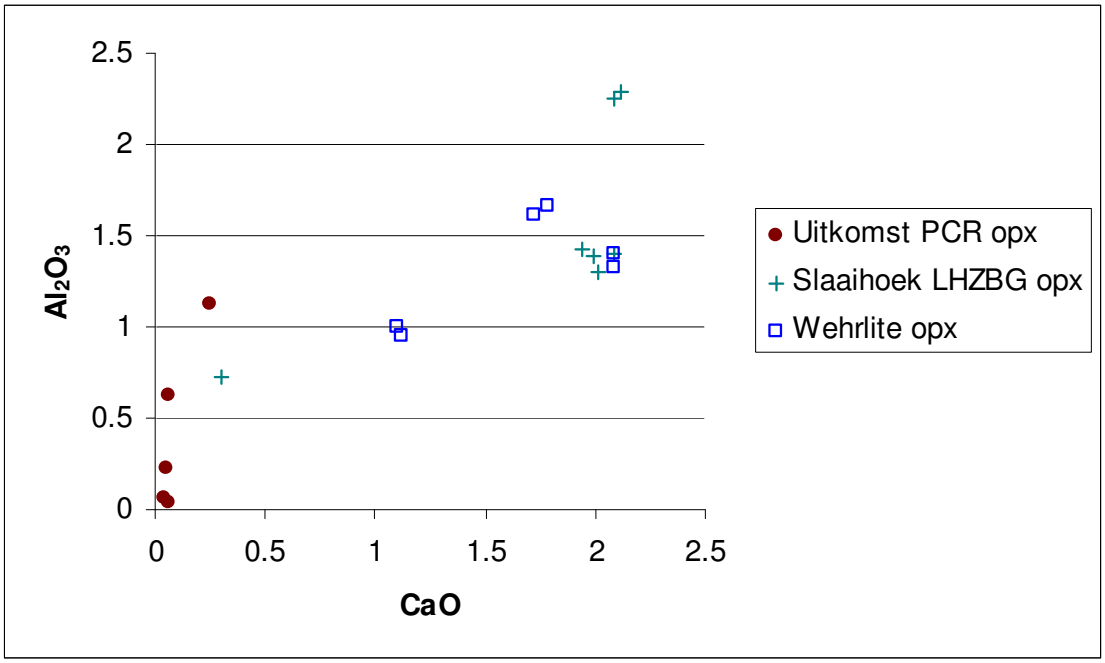

Figure 4.22. Al_2O_3 against CaO contents of orthopyroxenes analysed from the Uitkomst Complex.

The clinopyroxenes (Figure 4.21) from all of the occurrences have a near similar Al content, ranging from absent to 6 wt%. From the CaO content it may be seen that the clinopyroxene from the Uitkomst, PCR, wehrlite layers and Slaaihoek LHZBG has a slightly lower CaO content, but slightly higher Al_2O_3 content relative to the majority of clinopyroxene analyses from the Uitkomst LHZBG Unit and Uitkomst xenoliths. Some of the clinopyroxene grains from the Uitkomst LHZBG Unit show an increase in Al-content with decrease in Ca-content. There again appears to be a compositional "transitional" component from the higher Ca-clinopyroxene to the lower Ca-clinopyroxene variety. The enstatite from the Uikomst PCR Unit contains less Al than the orthopyroxene from the wehrlite layers and Slaaihoek LHZBG.

In Figure 4.22 the orthopyroxene compositions are compared in an Al_2O_3 versus CaO diagram. The enstatite from the Slaaihoek LHZBG and the wehrlite layers has a higher MnO content relative to the orthopyroxene found in the Uitkomst PCR harzburgite. The Slaaihoek LHZBG and wehrlite samples again seem to follow a general positive trend (Figure 4.22)

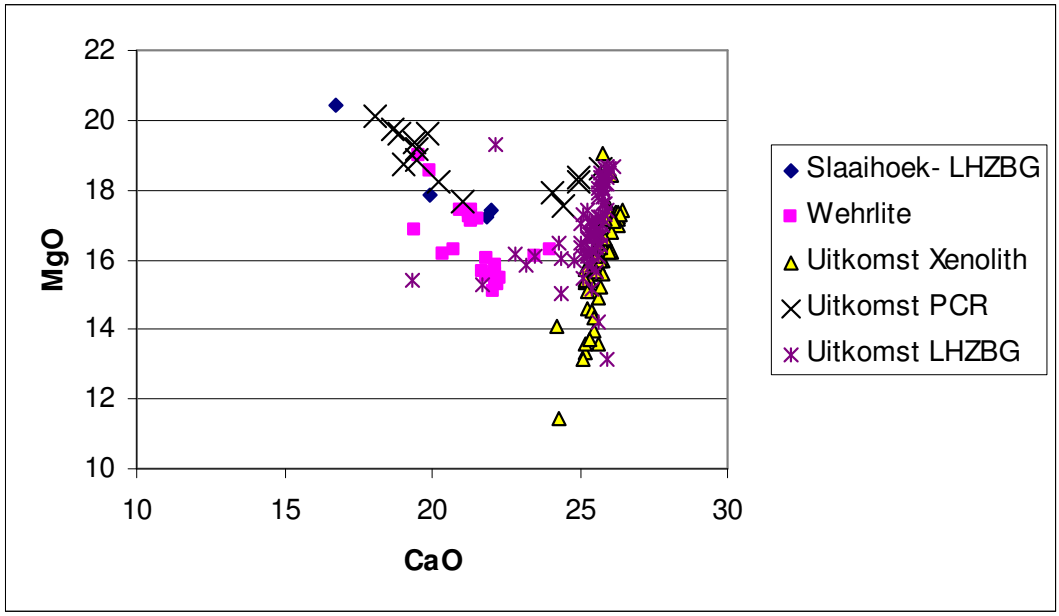

Figure 4.23. MgO versus CaO content of clinopyroxene grains analysed from the Uitkomst Complex.

In Figure 4.23 the clinopyroxene compositions are compared in an MgO versus CaO diagram. In the diopside samples from Slaaihoek LHZBG, wehrlite layers and Uitkomst PCR, there is a negative trend between MgO and CaO content. This may suggest substitution of Mg by Ca. This could be interpreted as indicative of a diopside forming in a dynamic magmatic environment, where a constant supply of mineral forming elements will be supplied. The Uitkomst xenolith and Uitkomst LHZBG diopside grain compositions do not show such a trend, indicative of possible substitution of elements, suggesting formation in a non-dynamic metamorphic environment, owing to depletion of mineral forming elements in the closed environment.

4.3 Plagioclase

Plagioclase was rarely encountered in the rocks sampled and was found to be present only in wehrlite layers within the LHZBG Unit, where it occurs in some samples as a minor mineral. The plagioclase shows evidence of saussuritization, but generally shows less evidence for alteration than the olivine and pyroxene (Figure 4.24). Microprobe analyses of the plagioclase indicated the grains to fall in the labradorite-bytownite compositional field (Steenkamp, 2004). The values correspond to those found by van Zyl (1996) and Gauert (1998).

Kacandes et al. (1989) did an experiment in which a quartz-normative tholeiite basalt (plagioclase, clinopyroxene, mesostasis and magnetite) was subjected to hydrothermal conditions at 300°C and 30 Mpa, and the evolution of the alteration minerals and fluid was monitored. It was found that the resultant secondary minerals, in order of detection were smectite, illite, potassium feldspar and cristobalite. This was followed by an examination of the unaltered minerals, demonstrating that the pyroxene and interstitial glass were the main source of cations, whereas the plagioclase appeared fresh. The fact that the plagioclase remained unaffected would suggest that either dissolution of the primary feldspars was slow or that the plagioclase was in near equilibrium with the fluid.

This would suggest that the near pristine plagioclase grains found in the LHZBG Unit were either in near equilibrium with the deuteric fluids that affected the surrounding precursor mafic minerals, or only suffered partial dissolution during the time it was exposed to the effects of the deuteric fluid.

Wenzel et al., (2001b) suggested that the assimilation of Ca from the country rock, resulted in the formation of Ca-Tschermak-rich interstitial clinopyroxene instead of plagioclase in the Ioko-Dovyren intrusion, Russia. This would suggest that the wehrlite layers represent pulses of primary mafic magma that were not affected by the assimilation of Ca from the dolomite country rock.

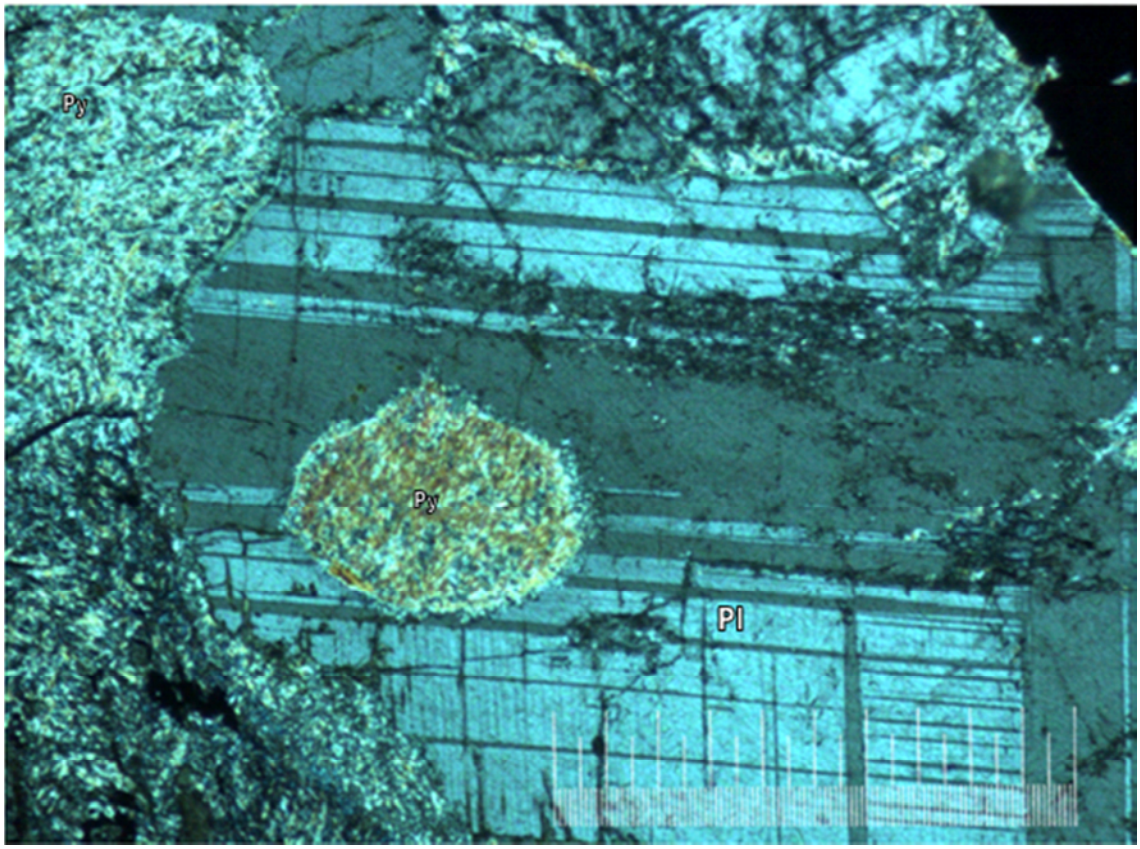

Figure 4.24. Plagioclase (Pl) that has been partially saussuritized. The plagioclase is both enclosing and being enclosed by completely uralitized pyroxene (py). The picture scale bar is 1000 microns. Taken with cross-polarised light. (Sample; CS18).

4.4 Chromite

4.4.1. Chromitite

Chromite is abundant in both the LHZBG and the PCR Units. In the LHZBG Unit chromite is found as disseminated grains and in thin seams within unaltered to altered peridotitic host material. The chromite grains in the LHZBG are usually euhedral and do not show the effects of alteration. The semi-massive chromitite mineralization in the PCR Unit is found in both a highly altered matrix material (Figure 4.25) and a less altered matrix material (Figure 4.26). The chromite grains in the PCR Unit are euhedral and show effects of alteration such as magnetite rims around grains and in cracks. Chromite compositional elements have been shown to be relatively immobile during hydrothermal processes, (Spandler et al. 2005) which may explain the preservation of chromite grains in completely altered matrices. The formation of the chromitite layers in the Uitkomst Complex has been attributed to an increase in oxygen fugacity within the evolving magma pile due to assimilation of dolomite (Gauert, 1998; Dodd, 2004).

Microprobe analyses of the centres of unaltered chromite grains in the PCR Unit reveal the compositional trends evident in Figures 4.27 and 4.28. The mineral chemistry of chromite grains encountered during this investigation, and obtained by electron microprobe analyses, is presented in Appendix 2.

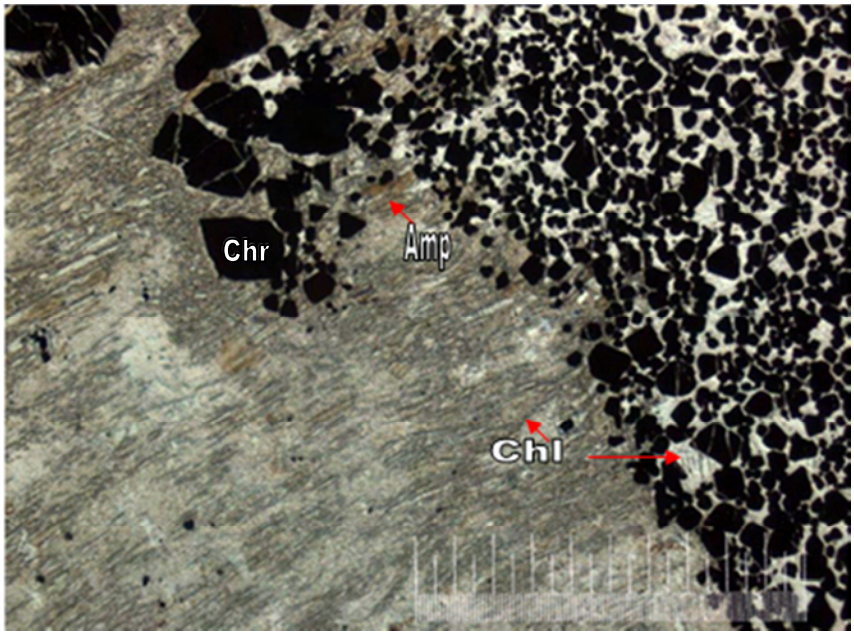

Figure 4.25. Euhedral to subhedral chromite (chr) grains in a matix of chlorite (chl) and relict amphibole (amp) from the PCR Unit. The picture scale bar is 1000 micron. Taken under cross-polarised transmitted light. (Sample: UK12A)

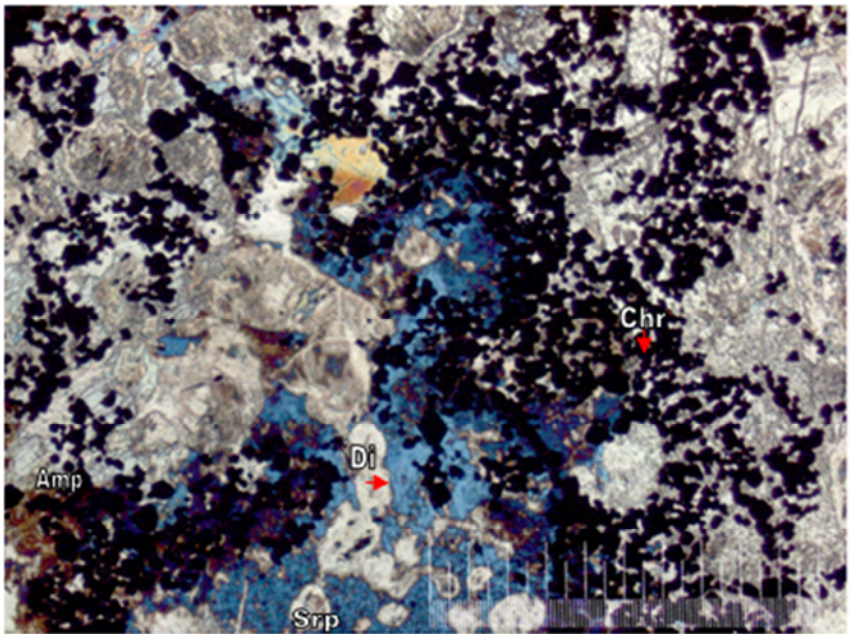

Figure 4.26. Euhedral grains of chromite (chr) (black) associated with serpentinized (srp) olivine and enclosed by diopside (di), partially altered to amphibole (amp), in the PCR Unit. The picture scale bar is 1000 microns. Taken under cross-polarised transmitted light. (Sample: UK12D).

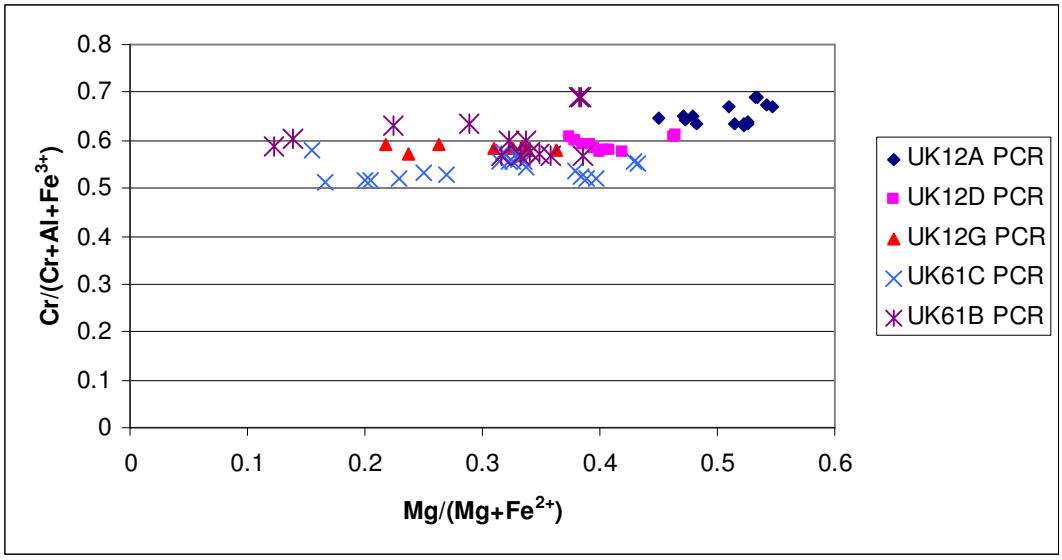

Figure 4.27. Cr/(Cr+Al+Fe^{3+}) against Mg/(Mg+Fe^{2+}) plot for chromite grains analysed from the PCR Unit.

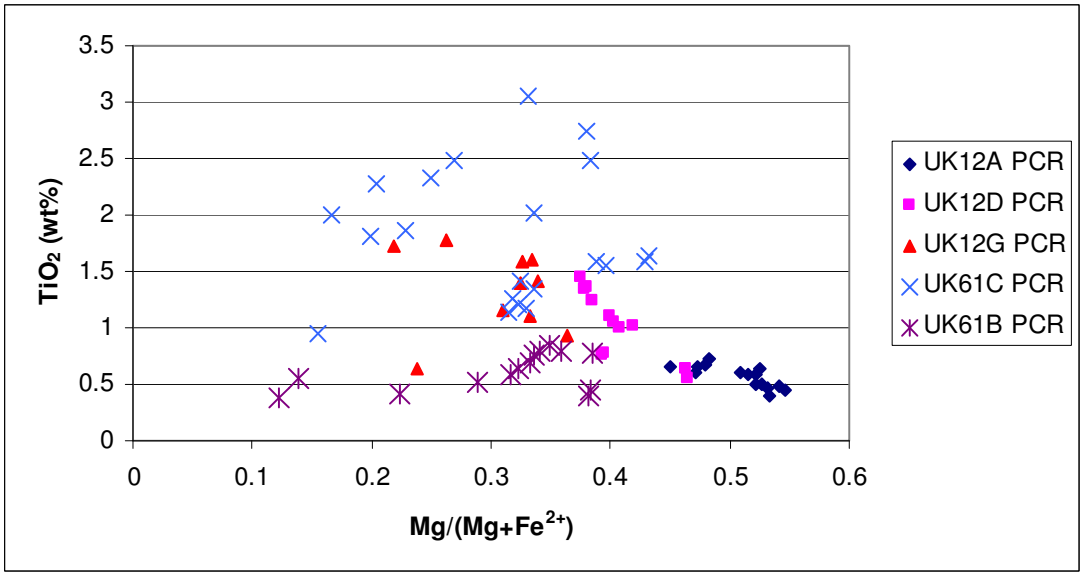

Figure 4.28. TiO2 (wt %) against Mg/(Mg+Fe^{2+}) plot for chromite grains analysed from the PCR Unit.

There is a systematic change in $Mg/(Mg + Fe^{2+})$ ratio in the PCR Unit with height (Figure 4.30), in borehole UK12 (where UK12A is near top, UK12D is near centre and UK12G is near the bottom of the unit). The $Mg/(Mg + Fe^{2+})$ ratio increases with height while the $Cr/(Cr + Al + Fe^{3+})$ ratio remains nearly constant. The same applies to borehole UK61. It can bee seen that the TiO_2 content decreases with height in borehole UK61 (Figure 4.28). The results are presented in Table 4.1.

Table 4.1. Comparison of chromite grains from the PCR Unit.

		UK12A	UK12D	UK12G	UK61B	UK61C
	n	15	12	10	14	21
Cr_2O_3 content		50.57	44.04	41.41	44.26	38.00
$Cr/(Cr+Al+Fe^{3+})$	mean	0.65	0.59	0.58	0.60	0.54
	std dev	0.02	0.01	0.01	0.04	0.02
$Mg/(Mg+Fe^{2+})$	mean	0.51	0.41	0.30	0.31	0.31
	std dev	0.03	0.03	0.05	0.08	0.08
TiO_2	mean	0.57	1.02	1.33	0.61	1.81
	std dev	0.09	0.28	0.35	0.16	0.57
Cr:Fe	mean	2.04	1.40	1.14	1.29	0.98
	std dev	0.16	0.14	0.04	0.21	0.17

The Student t-test of $Cr/(Cr+Al+Fe^{3+})$ between UK12A and UK12D yielded a result of 1.32575E-09, between UK12A and UK12G a result of 1.59595E-10 and between UK12D and UK12G a result of 0.043843546. The Student's t-test between UK61B and UK61C yielded a result of 0.000104066. The Student's t-test of $Mg/(Mg+Fe^{2+})$ between UK12A and UK12D yielded a result of 5.86317E-09, between UK12A and UK12G a result of 1.29744E-08 and between UK12D and UK12G a result of 4.296E-05. The Student's t-test between UK61B and UK61C yielded a result of 0.901223189.

4.5 Magnetite

4.5.1 General

Magnetite was encountered within various associations in the LHZBG and PCR Units. In summary, the magnetite is present in the following associations:

a) As secondary stringers associated with serpentinized cracks in olivine, or where the magnetite almost completely pseudomorphically replaces the olivine (Figure 4.29).
b) As secondary rims around sulphide grains, usually pyrrhotite, and along fractures in the sulphide grains.
c) As secondary rims around and along fractures in chromite grains (Figure 4.30).
d) Possibly as primary grains, that suffered alteration (silicification) due to late stage fluid infiltration. Preserved as chamosite pseudomorphs after the primary grains.

No primary magnetite was encountered during the current investigation, but was reported in previous studies (van Zyl, 1996). This would suggest that magnetite is not developed throughout the Uitkomst Complex. The secondary magnetite occurrence is described in the following chapter.

The only evidence of primary magnetite in the LHZBG unit is the pseudomorphs of chamosite after magnetite (Figure 4.29). Ilmenite is persevered as a trellis structure in these grains (Figure 4.30). Trellis structure ilmenite is characteristic of magmatic magnetite. These grains have prominent leucoxene rims where it is in contact with the surrounding pyrrhotite. These occurrences are limited to grain fully enveloped in pyrrhotite. These grains show evidence of having been affected by a late-stage secondary fluid. The host rock is hornblendite.

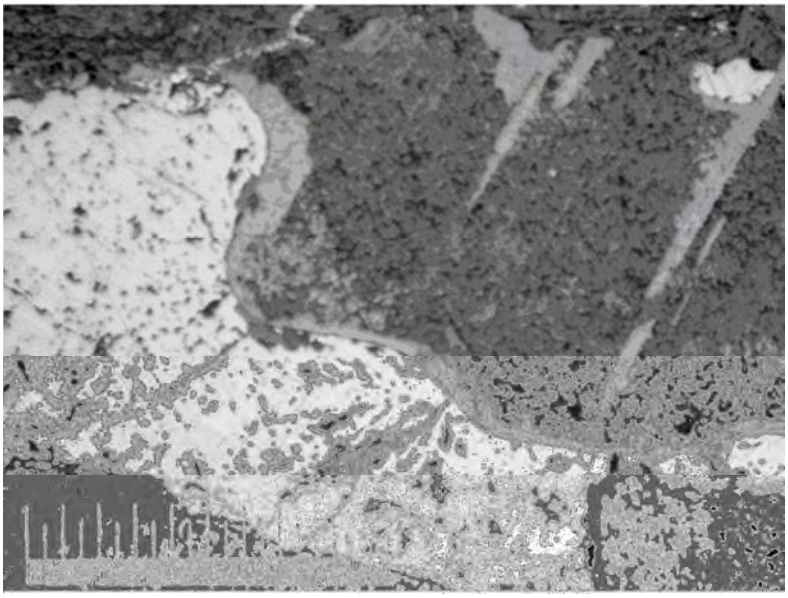

Figure 4.29. Pseudomorphs of chamosite (upper right) after primary magnetite with a leucoxene rim (light grey) and enveloped in pyrrothite (lower left). Photo taken under reflected light, scale bar = 1000 micron (Sample: UK48)

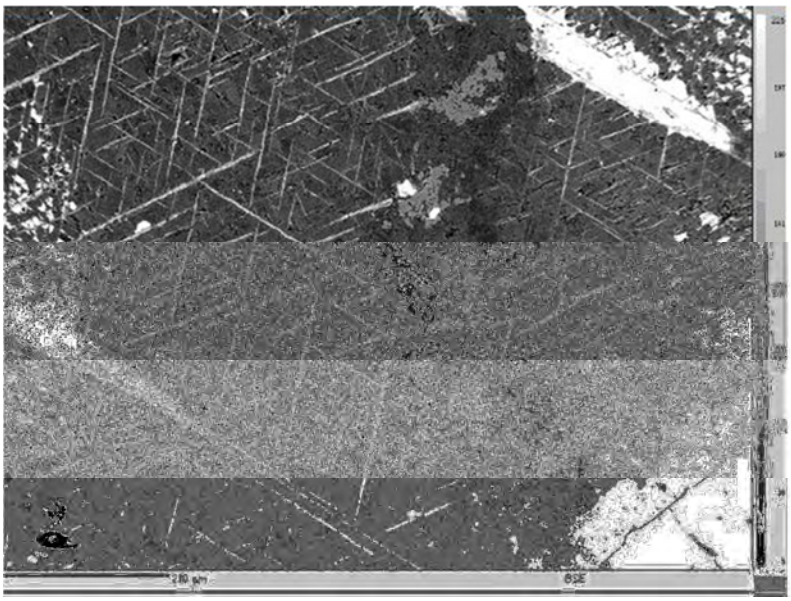

Figure 4.30. Backscatter electron (BSE) image of the preserved trellis structure of ilmenite in the chamosite pseudomorphs. A prominent alteration vein intrudes the grain (left of center in image). The leucoxene rim is visible in the lower left of the image where the grain is in contact with pyrrhotite. There are several pyrrhotite inclusions in the grain. The scale bar is 200 micron (Photo: P.P.H. Gräser).

4.7 Carbonate minerals

The carbonate minerals encountered during the investigation are calcite and dolomite. Calcite is found in the hybrid rocks and calc-silicate xenoliths of the LHZBG Unit. These two minerals are in textural equilibrium with the silicate and sulphide minerals. The carbonate minerals will be assumed to be primary in this context as representing relic primary country rock

4.7.1. Calcite

Where calcite is in contact with a sulphide grain (generally pyrrhotite), the contact is sharp and the sulphide minerals is not intergrown by tremolite often found in proximity to the sulphide mineralization (Figure 4.31).

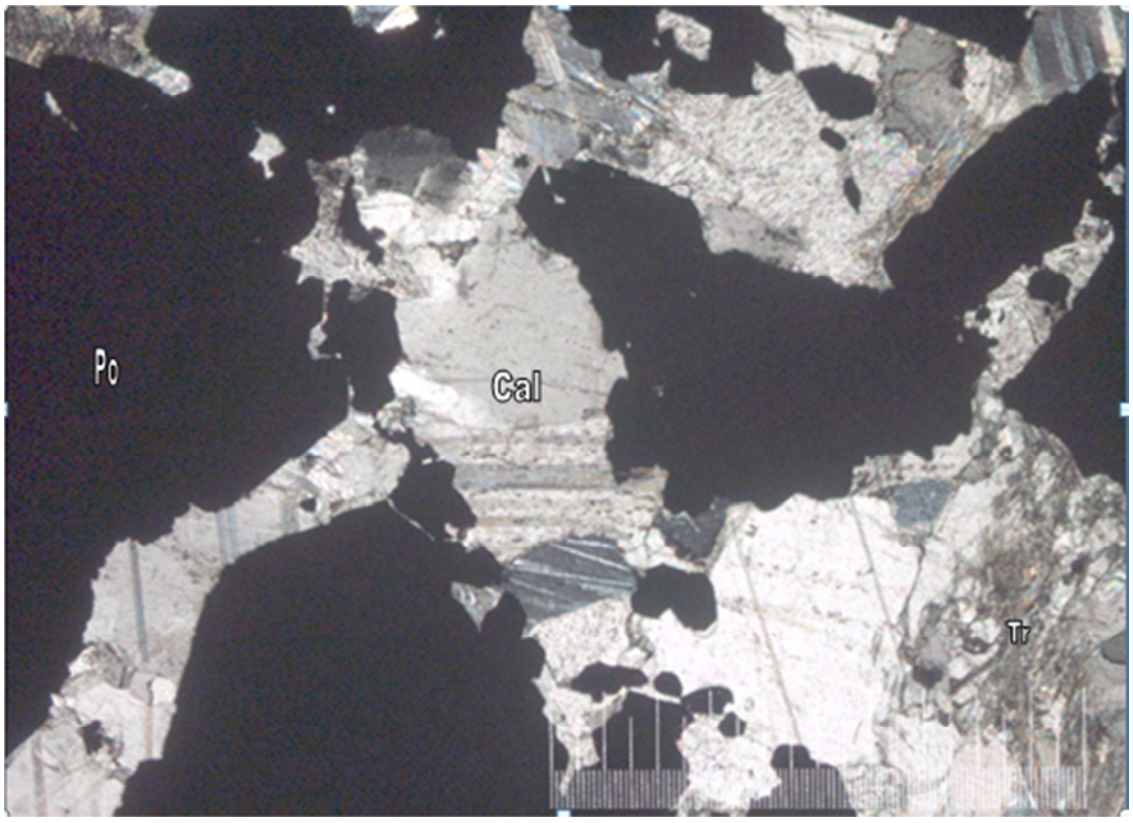

Figure 4.31. Calcite grains enclosing pyrrhotite (black) grains. The calcite (cal) grains appear to be in textural equilibrium with pyrrhotite (po) and tremolite (Tr). The picture scale bar is 1000 micron. Taken with cross-polarized light. (Sample; UK68E).

Calcite is also found in close association with tremolite in the hybrid rock of the LHZBG Unit (Figure 4.32), where the calcite grains are in textural equilibrium with tremolite and pyrrhotite grains.

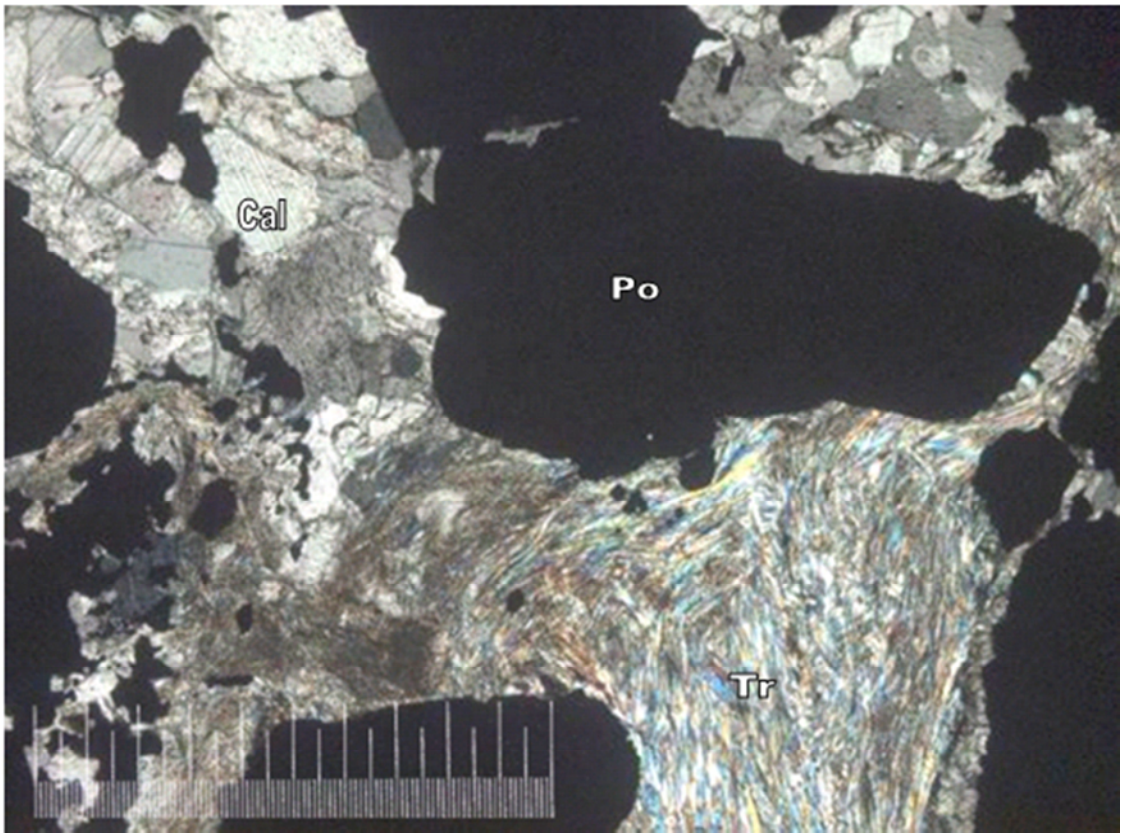

Figure 4.32. Calcite (Cal) and tremolite (Tr) appearing to be in textural equilibrium with each other and with pyrrhotite (Po) (black). The picture scale bar is 1000 microns and it was taken with cross-polarized light. (Sample: UK68E).

Grains of calcite were also found to be enveloped by sulphide in the hybrid rock of the LHZBG Unit (Figure 4.33). Some of the pyrrhotite appears to have infiltrated along the cleavage planes of the calcite grain.

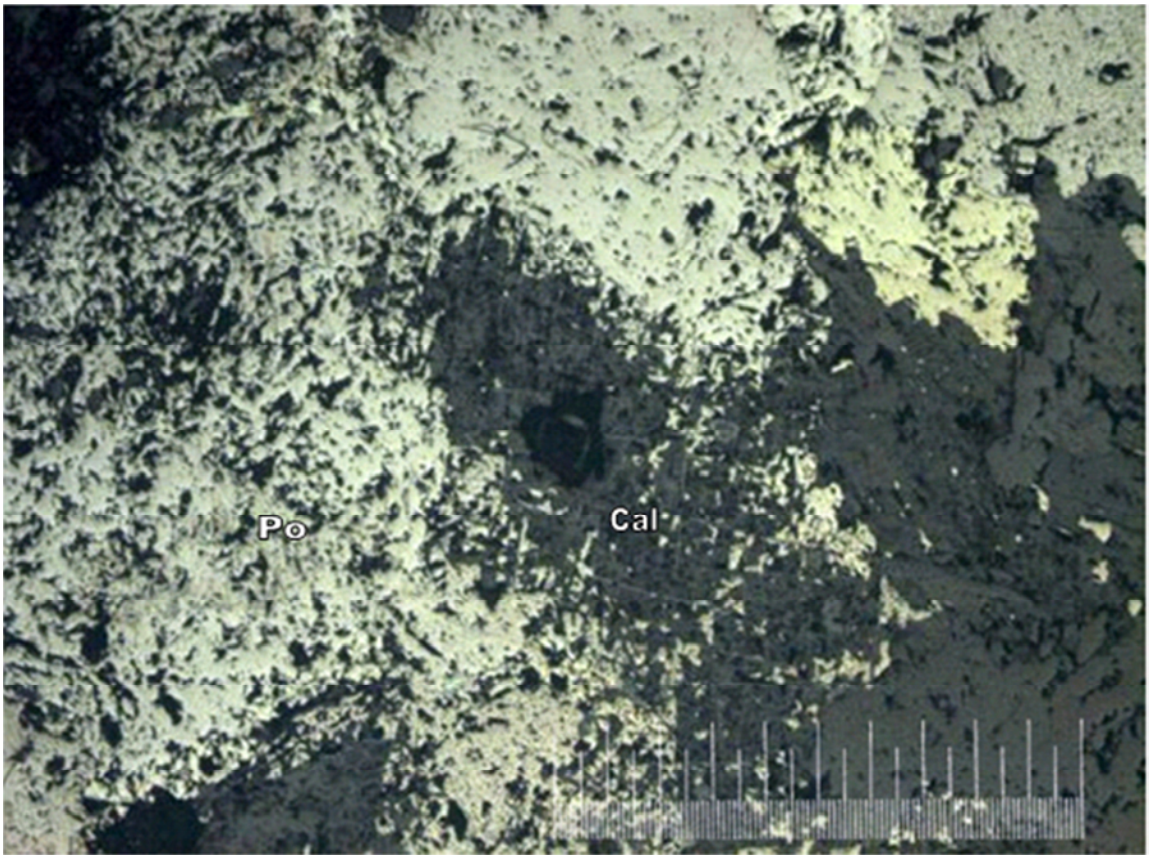

Figure 4.33. A calcite (Cal) grain (in centre of field of view) enveloped by pyrrhotite (Po). The picture scale bar is 1000 micron. Taken with reflected light. (Sample: UK48C).

In the calc-silicate xenoliths calcite encloses diopside grains (Figure 4.34) or occurs in thin veins. Clearly identifiable calcite grains are usually located away from the contact of the xenolith with the hybrid rock.

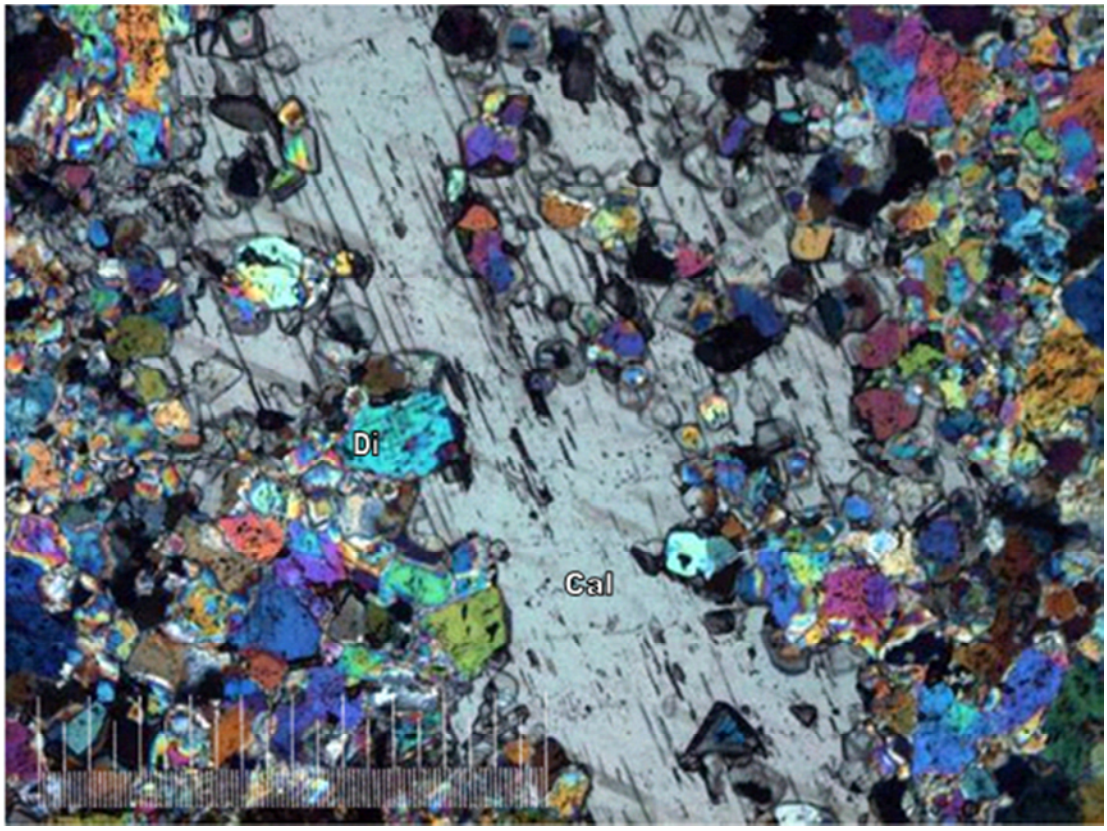

Figure 4.34. A large calcite (Cal) grain, in the center of the view, associated with diopside (Di) in a calc-silicate xenolith from the LHZBG Unit. The picture scale bar is 1000 micron. Taken with cross-polarized light. (Sample: UK3N).

4.7.2. Dolomite

Dolomite was encountered in association with talc, phlogopite and pyrite. The dolomite formed part of the assemblage dolomite-talc-phlogopite or is present as relic grains (Figure 4.35). Dolomite occurs in samples from both the PCR and LHZBG Units, close to the edge of the intrusion.

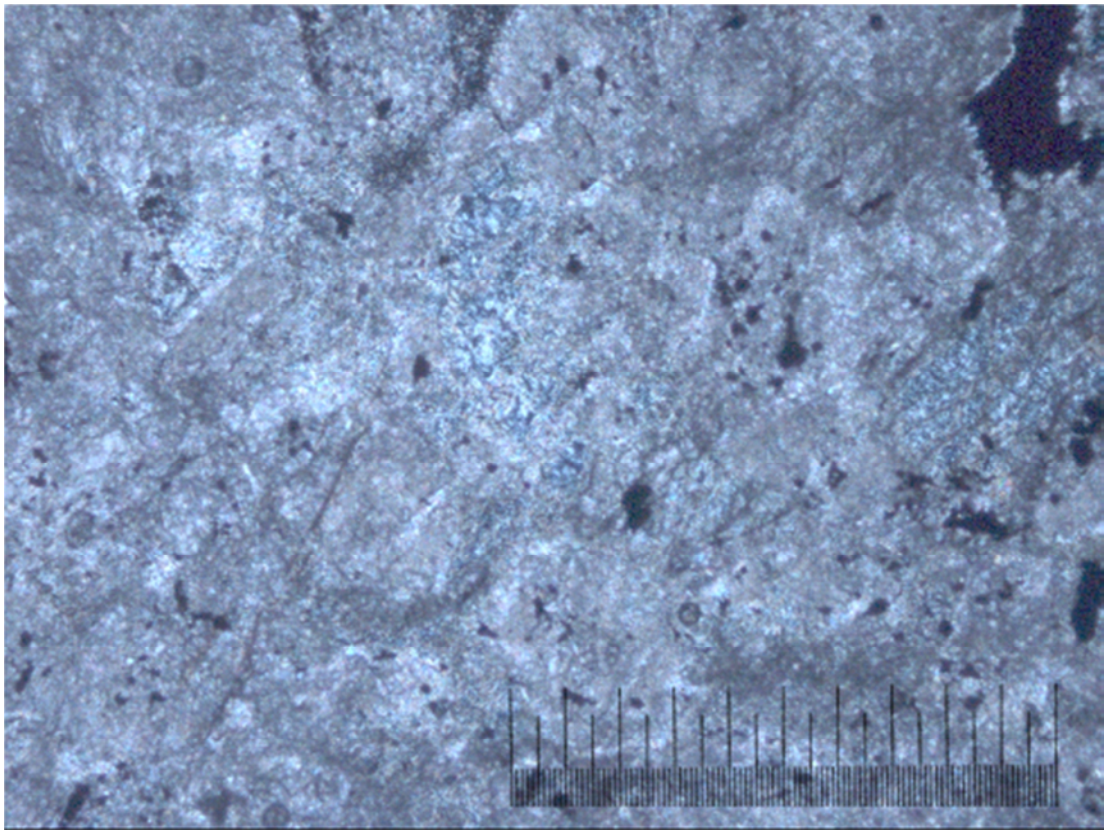

Figure 4.35. Dolomite grains (higher birefringence) occur along with talc and minor sulphides (black). The picture scale is 1000 microns. Taken with cross-polarized light. (Sample: UK61D).

In summary it may be stated that the calcite grains encountered during the investigation are only found in the LHZBG unit and are always in textural equilibrium with the surrounding minerals. In the calc-silicate xenoliths, calcite appeared as discrete, fine veins in close contact with diopside, away from the contact of the xenolith with the surrounding hybrid rock. The calcite grains in the hybrid rock are in textural equilibrium with both silicate (generally tremolite) and sulphide (generally pyrrhotite) minerals. Calcite grains partially enveloped by pyrrhotite are also present.